

Spherical Principal Curves

JANG-HYUN KIM, JONGMIN LEE AND HEE-SEOK OH

Seoul National University

Seoul 08826, Korea

Abstract: This paper presents a new approach for dimension reduction of data observed in a sphere. Several dimension reduction techniques have recently developed for the analysis of non-Euclidean data. As a pioneer work, Hauberg (2016) attempted to implement principal curves on Riemannian manifolds. However, this approach uses approximations to deal with data on Riemannian manifolds, which causes distorted results. In this study, we propose a new approach to construct principal curves on a sphere by a projection of the data onto a continuous curve. Our approach lies in the same line of Hastie and Stuetzle (1989) that proposed principal curves for Euclidean space data. We further investigate the stationarity of the proposed principal curves that satisfy the self-consistency on a sphere. Results from real data analysis with earthquake data and simulation examples demonstrate the promising empirical properties of the proposed approach.

Keywords: Dimension reduction; Feature extraction, Principal geodesic analysis; Principal curve; Spherical domain.

1 Introduction

A variety of dimension reduction techniques have been developed for representing and analyzing data. Most of the dimension reduction techniques are focused on Euclidean space data. Recently there has been a growing interest in the analysis of non-Euclidean data; some dimension reduction techniques for non-Euclidean data have been studied for shape analysis or motion analysis. For example, Siddiqi and Pizer (2008) and Cippitelli et al. (2016) considered a Cartesian product of $SO(2)$ (i.e., sphere) and \mathbb{R} for medial representation and skeleton data analysis, respectively. For these representations, existing

dimension reduction methods have been modified by considering geodesic distance. There have been several generalizations of principal component analysis (PCA) suited for non-Euclidean data, which contain Fletcher et al. (2004), Huckemann and Ziezold (2006), Huckemann et al. (2010), Jung et al. (2011), Jung et al. (2012), Panaretos et al. (2014), and Hauberg (2016). Fletcher et al. (2004) proposed a tangent plane approach of dimension reduction for manifold data, termed principal geodesic analysis (PGA). However, PGA is somewhat limited in scope because it can only perform the dimension reduction of spherical data onto the great circle. Along with this generalization, Jung et al. (2011) proposed a dimension reduction that extracts a circle on a sphere, and Jung et al. (2012) suggested principal nested spheres that can be considered as a high-dimensional version of Jung et al. (2011). Huckemann et al. (2010) suggested an extension of PCA using the intrinsic manifold structure and obtained their principal geodesic component as the best approximating the data does not necessarily pass through a predetermined intrinsic mean.

As a study that is closely related to our proposal, Hauberg (2016) developed principal curves on Riemannian manifolds. To be specific, Hauberg (2016) used an approximation to construct principal curves by a projection of the data onto the discrete points, unlike the original principal curve by Hastie and Stuetzle (1989) that projects the data onto a continuous curve. This approximation of finding closest points instead of projections on a curve causes a problem that may project different data points onto a single point mistakenly. In this study, we propose a new principal curve approach for spherical data by a projection of the data onto a continuous curve on a sphere instead of approximation, which improves dimension reduction and its stability. Our proposed approach is two-fold: One is the extrinsic approach that requires an additional space setting to the given manifold. In the case of the sphere, there exists a unique natural embedding space (three-dimensional space), and there is no question of the subjectivity of the extrinsic approach. The extrinsic approach is computationally efficient. The other is the intrinsic approach without any embedding space. Although this approach is difficult to calculate and impractical (Srivastava and Klassen, 2002), it is necessary to develop principal curves to a generic manifold. Furthermore, we investigate the stationarity of spherical principal curves obtained by both proposed approaches.

To sum up, the main contributions of this study can be summarized as follows: (a) We present a new principal circle defined on a sphere for initialization of the proposed principal curves. (b) We propose both extrinsic and intrinsic approaches to construct principal curves on a sphere. (c) We develop median principal curves that might be resistant to outliers, which can be considered as a robust extension of the proposed principal curves. (d) We verify the stationarity of all the proposed principal curves on the sphere.

The remainder of this paper is organized as follows. Section 2 briefly reviews conventional principal curves and intrinsic and extrinsic means on manifolds. In Section 3, a newly developed exact principal circle on a sphere is studied, which is used for the initialization of the proposed principal curves. Section 4 presents the proposed principal curves with a practical algorithm and investigates the stationarity of them theoretically. In Section 5, the experimental results of the proposed method are provided through earthquake data from the U.S. Geological Survey and simulation examples. Section 6 discusses a robust extension of intrinsic principal curves, termed median principal curves. Finally, concluding remarks are given in Section 7. The detailed proofs of properties of the principal curve on the sphere are given in Appendix.

Before closing this section, we remark that, as a significant extension of canonical interpretation of principal component analysis on Riemannian manifolds, Panaretos et al. (2014) introduced a smooth curve on the manifold, termed principal flow, which passes through the mean of given data and allows for non-geodesic flexibility of curve fitting of the data. Along with this line, the concept of principal flows can be shared with that of our method. Nevertheless, in this study, we focus on a direct extension of principal curves from Euclidean space to Riemannian manifolds, such as a sphere.

2 Backgrounds

2.1 Principal Curves

Principal curves of Hastie and Stuetzle (1989) can be considered as a nonlinear generalization of PCA that finds an affine space that maximizes the variance of the projected data. The curve is a function from a one-dimensional closed interval to a given space, and

further, curve f is said to be self-consistent or a principal curve of X if the curve satisfies

$$f(\lambda) = E(X | \lambda_f(X) = \lambda), \quad (1)$$

where $f(\lambda_f(x))$ is the projection of the point x to the function f . It implies that $f(\lambda)$ is the average of all data points projected onto $f(\lambda)$ itself. One of the most important consequences of self-consistency is that the principal curve is a critical point of the reconstruction error for small perturbations (Hastie and Stuetzle, 1989).

The existence of principal curves satisfying the self-consistency for a given distribution is not guaranteed. It is also difficult to formulate the principal curve by solving the self-consistent equation of (1). Thus, by the algorithm of Hastie and Stuetzle (1989), we set the principal curve as the first order spline connected by T points, where the points are initialized by the given rule. The T points of the principal curve are updated so that the curve reaches the self-consistency condition by iterating the following two steps, projection and expectation: (a) In the projection step, the given data are projected onto the curve. If the projection index is not unique, it is set to be the maximum value among them. (b) In the expectation step, the curve is updated to satisfy the self-consistency.

In practice, the projection indices of the data are likely to be different. Thus, each point of the curve is updated to the local weighted mean of data points projected near the point of the curve. These two steps are iterated until the reconstruction error is converged.

As related works, Banfield and Raftery (1992) proposed a modification of the original algorithm by Hastie and Stuetzle (1989) to reduce bias when segments of function f have high curvature. Tibshirani (1992) presented a different definition of principal curves based on a mixture model and suggested an EM algorithm for estimation to reduce bias.

2.2 Means on Manifolds

The self-consistency of principal curves on Euclidean space implies that the conditional expectation of random variable X given a projection index coincides with the point of the curve at the projection index. On the one hand, the concept of the expected value of a distribution is expandable in a smooth manifold and is called as *Fréchet mean*. Given a probability distribution Q on a smooth Riemannian manifold M with a distance $\rho(\cdot, \cdot)$,

the Fréchet mean $m \in M$ is defined as

$$\arg \min_{m \in M} \int \rho^2(m, x) Q(dx). \quad (2)$$

The natural distance on a manifold is geodesic distance $d_{Geo}(\cdot, \cdot)$. The Fréchet mean of (2) using d_{Geo} as distance is termed as *intrinsic mean* (Bhattacharya and Patrangenaru, 2003). However, in general, it is difficult to solve geodesic distance and to ensure the uniqueness of intrinsic mean (Le and Kume, 2000).

On the other hand, by embedding a given manifold M into a higher dimensional Euclidean space \mathbb{R}^p , the Fréchet mean can be calculated using Euclidean distance in \mathbb{R}^p , which is called as *extrinsic mean*. With letting ξ denote embedding from M to \mathbb{R}^p , the extrinsic mean is defined as

$$\arg \min_{m \in M} \int \|\xi(m) - \xi(x)\|^2 Q(dx). \quad (3)$$

It is equivalent to the projection of the mean value of data points in \mathbb{R}^p to M (Bhattacharya and Patrangenaru, 2003). With a projection mapping $\pi : \mathbb{R}^p \rightarrow M$ as $\pi(y) = \arg \min_{m \in M} \|\xi(m) - y\|$, the extrinsic mean of (3) can be calculated as

$$\text{extrinsic mean} = \pi \left(\int \xi(x) Q(dx) \right). \quad (4)$$

We remark that the extrinsic mean obtained by Euclidean distance holds a computational advantage, compared to the intrinsic mean (Bhattacharya et al., 2012). Moreover, the extrinsic mean is indistinguishable from the intrinsic mean in the case that the distribution has support in a small region (Bhattacharya and Patrangenaru, 2005).

2.3 Existing Principal Curves on Riemannian Manifolds

Hauberg (2016) developed principal curves on Riemannian manifolds by extending the previous work of Hastie and Stuetzle (1989). The principal curve by Hauberg (2016) is represented as a set of points, $f = \{C_1, \dots, C_T\}$, joined by geodesic segments. These points are initialized with the principal geodesic. The fitting algorithm of the curves follows that of Hastie and Stuetzle (1989). More specifically, the mean operation in the expectation

step of Hastie and Stuetzle (1989) is replaced with the intrinsic mean, and in the projection step, each data point is projected onto the closest points in f as

$$\text{proj}(x) = \arg \min_{C_i \in f} d_{Geo}(x, C_i).$$

Note that Hauberg’s algorithm does not perform accurate projection on a principal curve.

3 Enhancement of Principal Circle for Initialization

In this section, we improve the principal circle to use the initialization for the proposed principal curves in Section 4.

3.1 Principal Geodesic and Principal Circle

The principal curve algorithm of Hastie and Stuetzle (1989) uses the first principal component as the initial curve, which is easily calculated by singular value decomposition (SVD) of the data matrix in Euclidean space. Along with this line, the proposed principal curve algorithm in Section 4 requires an initial curve.

Principal geodesic analysis (PGA) by Fletcher et al. (2004) can be considered as a generalization of PCA, which performs dimension reduction of data on the Cartesian product of simple manifolds. For this purpose, Fletcher et al. (2004) projected each manifold component of data onto the tangent space at the intrinsic mean of each component. As a result of the tangent space approximation of each component, the given data are approximated by points on Euclidean space; thus, by applying PCA, the dimension reduction can be performed through the inverse process of the tangent projection. For a spherical case, they particularly perform tangent space projection using an inverse exponential map, which is called as *log map*. The log map at $(0,0,1)$ of the unit sphere centered at the origin of \mathbb{R}^3 is given by Fletcher et al. (2004) as

$$\text{log map}_{(0,0,1)}(x_1, x_2, x_3) = \left(x_1 \frac{\theta}{\sin \theta}, x_2 \frac{\theta}{\sin \theta} \right),$$

where (x_1, x_2, x_3) is a point on the unit sphere and $\theta = \arccos(x_3)$.

Principal curves on manifolds by Hauberg (2016) employ PGA for the initialization of a curve without endpoints and use a circle by tangent approximation for initialization of a

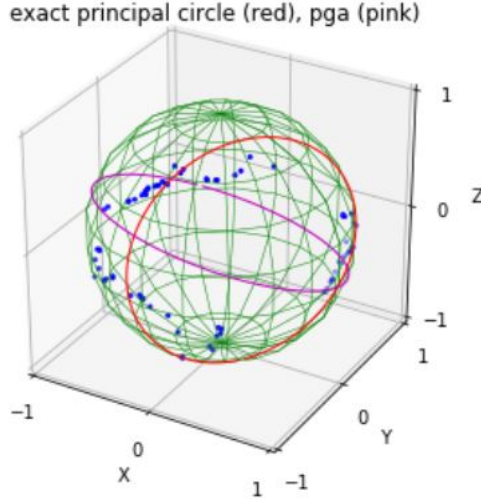


Figure 1: Spherical distribution of significant earthquakes, the result (pink) by PGA, and the result (red) by our proposed principal circle.

closed curve. The first principal component obtained by the projection of manifolds into the tangent space corresponds to the geodesic in the existing manifolds (Fletcher et al., 2004). Thus, principal curves by Hauberg (2016) are initialized as great circles or approximated circles that do not minimize a reconstruction error for the representation of spherical data. However, geodesic on a sphere is limited to represent data on the sphere. Figure 1 shows earthquake data from the U.S. Geological Survey that represent the locations (blue dots) of significant earthquakes of Mb magnitude 8+ around the Pacific ocean since 1900. The data will be analyzed detailedly Section 5. In Figure 1, the result (pink) by PGA does not fit the data appropriately, while our principal circle (red) in Section 3.2 improves the representation of the data.

In literature, there exists an attempt by Jung et al. (2011) that generalizes PGA to a circle on a sphere. The circle on the sphere that minimizes a reconstruction error is called *principal circle*, where the reconstruction error is defined as the total sum of squares of geodesic distances between curve and data. Jung et al. (2011) used a doubly iterated algorithm that finds the principal circle after projecting the data onto the tangent space by using the log map. However, this approach suffers from two problems. First, using the tangent approximation in minimizing the distance causes numerical errors. In the case that

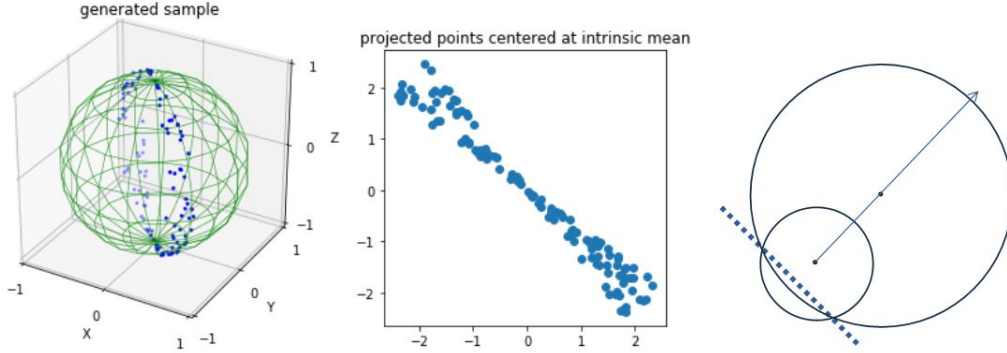


Figure 2: (Left) Simulated data points that are located in longitudes $[0.7, 0.8]$ with the intrinsic mean $(0, 0, 1)$. (Middle) The projected points from the sphere onto the tangent plane at $(0, 0, 1)$. (Right) A case that the principal circle does not exist.

data points are located far away from the mean, the numerical errors increase considerably because there is no local isometry between the sphere and its tangent plane from the *Gauss's Theorema Egregium*. For instance, the left panel in Figure 2 shows simulated data distributed in the range of longitudes from 0.7 to 0.8, where the underlying structure is a great circle. Suppose that the intrinsic mean of the dataset is $(0, 0, 1)$. It means that even if the structure is a circle, data points are mainly concentrated on around the north pole, which looks like an inhomogeneous great circle. The middle panel shows projected points of the dataset onto the tangent plane at $(0, 0, 1)$. Although the data points around the south pole are dense, they become somewhat scattered after mapping onto the plane, as shown in the middle panel, which causes numerical errors (non-isometricity). Secondly, owing to a topological difference between sphere and plane, the existence of principal circles in the plane is not guaranteed. Even though the sphere is compact, the tangent plane is not compact, merely open. From the compactness of the sphere, the least square circle always exists regardless of the data structure; however, it does not work in the plane. In the right panel of Figure 2, the blue dotted points are the projected ones onto the plane, which form a non-periodic line. Because a small arc of a big circle looks like a line, there are infinitely many circles that minimize the reconstruction error to be sufficiently close to 0. Hence, the least square circle does not exist in this case.

In this study, for a better initialization of the proposed principal curves in Section

4, we propose a new principal circle that does not depend on tangent projection. This attempt was previously made by Gray et al. (1980), which embeds a sphere into three-dimensional space and then find a circle that minimizes the reconstruction error through an iterative quadratic approximation of geodesic distances in the three-dimensional spatial coordinate system. Specifically, Gray et al. (1980) expressed the center of the circle as three-dimensional coordinates (x_1, x_2, x_3) with a constraint of $x_1^2 + x_2^2 + x_3^2 = 1$.

On the other hand, we obtain the constraint-free optimization problem by expressing the center of the circle using a spherical coordinate system in Section 3.2; hence, our principal curve can be obtained through a simple algorithm.

3.2 Intrinsic Principal Circle

For our principal circle, we consider an intrinsic optimization algorithm that does not use an approximation; thus, it is simple and is applicable to some situations focused on a two-dimensional sphere instead of a high-dimensional one. Let $d_{Geo}(x, y)$ denote the minimal geodesic distance between two points x and y on a sphere. For a given dataset D and a circle C on a sphere, let $\delta(D, C)$ be the sum of squares of distances between circle and data, defined as

$$\delta(D, C) = \sum_{x \in D} d_{Geo}(x, \text{proj}_C(x))^2,$$

where $\text{proj}_C(x)$ denotes a projection of x on C . The goal is to find a circle C on the sphere that minimizes $\delta(D, C)$. To solve this optimization problem, we represent a circle C by a center c of the circle and a radius $r \in [0, \pi]$ that is a geodesic distance between the center c and the circle C . This representation is not unique. For example, let c' be the antipode of c , then (c, r) and $(c', \pi - r)$ represent the same circle C . Nevertheless, it is not crucial to the optimization problem since we simply find a representation of the least square circle. See Figure 3. By using a spherical coordinate system, it is able to parameterize c as (θ, ρ) , where θ denotes the azimuth angle and ρ is the polar angle. By symmetricity of the circle, $d_{Geo}(x, \text{proj}_C(x))$ can be easily calculated by

$$d_{Geo}(x, \text{proj}_C(x)) = d_{Geo}(x, c) - r.$$

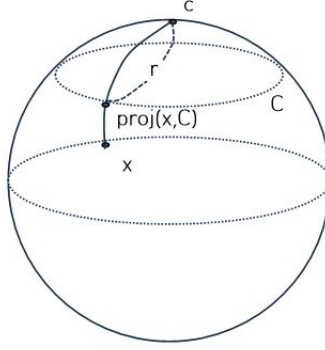


Figure 3: $d_{Geo}(x, \text{proj}_C(x))$ is expressed as $d_{Geo}(x, c) - r$.

Thus, we have

$$\delta(D, C) = \sum_{x \in D} (d_{Geo}(x, c) - r)^2. \quad (5)$$

With letting $c = (\theta_c, \rho_c)$ and $x = (\theta_x, \rho_x)$ in the spherical coordinate system, the geodesic distance $d_{Geo}(x, c)$ is given by the spherical law of cosines with three points c , x and the polar point (see Appendix for details)

$$d_{Geo}(x, c) = \arccos(\cos \rho_c \cos \rho_x + \sin \rho_c \sin \rho_x \cos(\theta_c - \theta_x)). \quad (6)$$

By putting (6) into (5), it follows that $\delta(D, C)$ is represented as a three-parameter differentiable function $\delta_D(\theta_c, \rho_c, r)$ in domain $S^1 \times S^1 \times [0, \pi]$. Since $S^1 \times S^1 \times [0, \pi]$ is compact, the function $\delta_D(\theta_c, \rho_c, r)$ holds global minimum value; hence, it can apply the gradient descent method to find the solution. Here is the algorithm to find a principal circle by the above description.

Algorithm 1 Intrinsic Principal Circle by Gradient Descent

```

Initialize  $(\theta_c, \rho_c, r)$  as  $(\bar{\theta}, \bar{\rho}, \pi/2)$ 
while  $(\Delta\delta(D, C) \geq \text{threshold})$  do
     $(\theta_c, \rho_c, r) \leftarrow (\theta_c, \rho_c, r) - \beta \nabla \delta_D(\theta_c, \rho_c, r)$ 
end while

```

Notice that the algorithm can converge to a local minimum since $\delta_D(\theta_c, \rho_c, r)$ is not a convex function. Therefore, the intrinsic mean of the data set D is recommended for

the initial setting. Denote $(\bar{\theta}, \bar{\rho})$ as spherical coordinates of the intrinsic mean. Besides, β denotes the step size of the algorithm, which works well unless β is too large.

4 Proposed Principal Curves

In this section, we propose both extrinsic and intrinsic principal curves on a sphere and present practical algorithms for implementing the procedures. We further investigate the stationarity of the proposed principal curves.

4.1 Extrinsic Principal Curves

As mentioned previously, Hauberg’s algorithm does not perform exact projection on a principal curve. On the other hand, when we focus on a sphere, by using the series of rotations, it is able to perform exact projection on the geodesic segments, and hence, obtain a continuous and sophisticated dimension reduction, which is our main feature that is distinguished from Hauberg’s principal curves. Like the original one of Hastie and Stuetzle (1989), we consider performing the projection and expectation steps iteratively to obtain principal curves on a sphere.

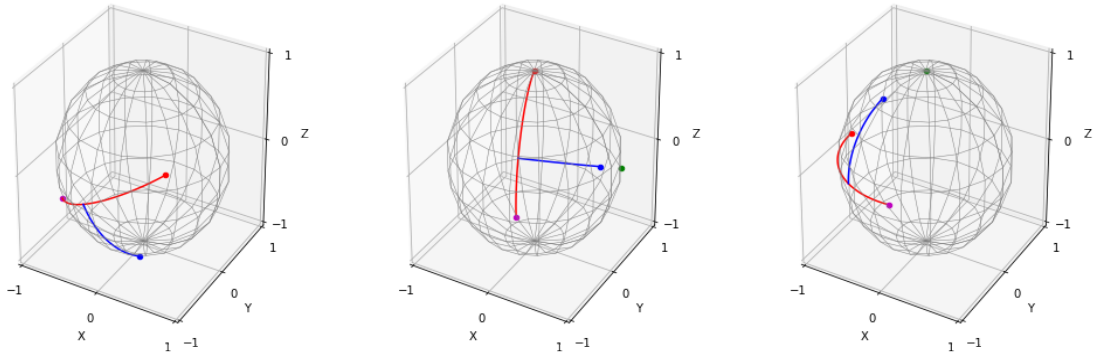


Figure 4: Projecting a point (blue) onto the geodesic segment (red) by using rotations. (Left) Initial position of the point and the geodesic segment. (Middle) Rotating one of the end points of the geodesic segment to the north pole. (Right) Rotating the center of the circle to the north pole.

In the projection step, each data point is projected on the curve along a geodesic. To

project a point on an arbitrary geodesic segment, we rotate the geodesic segment to be aligned on the equator. Next, we project the rotated data point on the rotated geodesic segment and re-rotate the result to get coordinates of the projection that we want. Figure 4 shows this procedure that projects a point to the geodesic segment by using rotations. In the left panel of Figure 4, the initial position of the point (blue) and the corresponding geodesic segment (red) are displayed. The middle panel shows a rotated result obtained after rotating one of the endpoints of the geodesic segment to the north pole. As a result of this rotation, the geodesic becomes a part of a great circle perpendicular to the xy -plane. By adding $\pi/2$ to the azimuth angle of the geodesic, it is able to get the center (green) of the great circle, which contains the geodesic segments. The right panel shows a rotated result from rotating the center of the circle to the north pole. As one can see, the geodesic segment is now aligned on the equator, so we can easily calculate the coordinates of projection from the point (blue) using a spherical coordinate system. By the inverse process of these rotations, we obtain the coordinates of the projection in the original coordinate system. Finally, after projecting the data point on each geodesic segment of the principal curve, we obtain the projection on the curve by choosing the closest geodesic segment. Let $\lambda_f(x)$ denote the projection index of a point x to the curve $f(\lambda)$, where $\lambda \in [0, 1]$. Then, the projection of x can be expressed as

$$\text{projection of } x = f(\lambda_f(x)), \quad \lambda_f(x) = \arg \min_{\lambda} d_{Geo}(x, f(\lambda)).$$

In the expectation step, we find the mean of data points. Mean on a sphere can be obtained from both intrinsic and extrinsic perspectives. We first focus on the extrinsic approach. The extrinsic approach is advantageous in that it has a smaller computational complexity compared to the intrinsic algorithm, and further, the stationarity of the spherical principal curves can be held. The expectation step follows that of the principal curve of Hauberg (2016), i.e., updating the weighted average by smoothing that makes the curve closer to the self-consistency condition. Suppose that we have n data points $\{x_i\}_{i=1}^n$ and the corresponding projection indices $\{\lambda_i\}_{i=1}^n$, where $\lambda_i = \lambda_f(x_i)$ for $i = 1, \dots, n$. Let T denote the number of points in an initial curve. The local weighted smoother updates the t th point of the principal curve C_t with the weighted extrinsic mean of data points for $t = 1, \dots, T$.

We use a quadratic kernel $k(\lambda) = (1 - \lambda^2)^2 \cdot \delta_{|\lambda| \leq 1}$, as Hauberg (2016), and the weights are given by $w_{t,i} = k(|\lambda_f(C_t) - \lambda_i|/\sigma)$, where $\sigma = q \cdot \text{length of curve}$ for fixed q .

Here are the detailed steps for obtaining the proposed extrinsic principal curve.

Algorithm 2 Extrinsic Principal Curve

1. Initialize principal curve $f = \{C_1, \dots, C_T\}$ as principal circle.
 2. Parameterize the curve as $f(\lambda)$ by the unit speed in the geodesic distance.
 3. Do projection $\lambda_f(x_i) = \arg \min_{\lambda} d_{Geo}(x_i, f(\lambda))$, $i = 1, \dots, n$.
 4. Calculate $\delta(D, f) = \sum_{i=1}^n d_{Geo}^2(x_i, f(\lambda_f(x_i)))$.
- while** $(\Delta\delta(D, f) \geq \text{threshold})$ **do**
- Expectation $C_t = \sum_{i=1}^n w_{t,i} x_i / \|\sum_i w_{t,i} x_i\|$, $t = 1, \dots, T$.
 - Reparameterize the curve as $f(\lambda)$ by the unit speed in the geodesic distance.
 - Projection $\lambda_f(x_i) = \arg \min_{\lambda} d_{Geo}(x_i, f(\lambda))$, $i = 1, \dots, n$.
 - Calculate $\delta(D, f) = \sum_{i=1}^n d_{Geo}^2(x_i, f(\lambda_f(x_i)))$.
- end while**
-

We remark that, for principal curves on a sphere, we can choose the curves to have either the endpoints or not. Through our experiments, we observe that there is no significant difference in empirical performance. As far as Euclidean space is concerned as embedding space, the extrinsic approach is advantageous in computational efficiency. However, if data points, in the expectation step, are not contained in local regions, then the intrinsic way may have better performances than the extrinsic one. Moreover, the intrinsic manner might be appealing owing to its inherent metric.

4.2 Intrinsic Principal Curves

Intrinsic principal curves can be obtained by using the intrinsic mean in the expectation step of Algorithm 2. In our case, the intrinsic mean is the point that minimizes the sum of square of the geodesic distances $\sum_{x \in \text{data}} d_{Geo}^2(x, \cdot)$; thus, the minimum cannot be solved explicitly; instead, it can be approximately obtained by an iterative algorithm (Fletcher et al., 2004). Although the intrinsic mean exists due to the compactness of the sphere, uniqueness is guaranteed only in a restricted region. Specifically, the intrinsic mean is

determined uniquely for a random vector X on the unit sphere S^2 satisfying $d_{Geo}(X, p) < \frac{\pi}{2}$ for some $p \in S^2$ (Pennec, 2006).

Here are the detailed steps for obtaining the proposed intrinsic principal curve.

Algorithm 3 Intrinsic Principal Curve

1. Initialize principal curve $f = \{C_1, \dots, C_T\}$ as principal circle.
 2. Parameterize the curve as $f(\lambda)$ by the unit speed in the geodesic distance.
 3. Do projection $\lambda_f(x_i) = \arg \min_{\lambda} d_{Geo}(x_i, f(\lambda))$, $i = 1, \dots, n$.
 4. Calculate $\delta(D, f) = \sum_{i=1}^n d_{Geo}^2(x_i, f(\lambda_f(x_i)))$.
- while** $(\Delta\delta(D, f) \geq \text{threshold})$ **do**
- Expectation $C_t = \arg \min_x \sum_{i=1}^n w_{t,i} \cdot d_{Geo}^2(x, x_i)$, $t = 1, \dots, T$.
 - Reparameterize the curve as $f(\lambda)$ by the unit speed in the geodesic distance.
 - Projection $\lambda_f(x_i) = \arg \min_{\lambda} d_{Geo}(x_i, f(\lambda))$, $i = 1, \dots, n$.
 - Calculate $\delta(D, f) = \sum_{i=1}^n d_{Geo}^2(x_i, f(\lambda_f(x_i)))$.
- end while**
-

4.3 Stationarity of Principal Curves

For a random vector X on \mathbb{R}^p for $p \in \mathbb{N}$, the stationarity of the principal curve of X is given by Hastie and Stuetzle (1989) as

$$\left. \frac{dE_X d^2(X, f + \epsilon g)}{d\epsilon} \right|_{\epsilon=0} = 0, \quad (7)$$

where f and g are smooth curves on \mathbb{R}^p satisfying $\|g\| \leq 1$ and $\|g'\| \leq 1$, and $d(X, f)$ denotes the distance from X to the curve f .

However, unlike \mathbb{R}^p , it is not easy to define addition on a sphere. Thus, it is necessary to redefine some concepts, such as addition and perturbation, in order to extend the properties of the principal curves on Euclidean space to a spherical surface. We conversely consider $f + g$ ($:=h$) firstly, instead of g . Specifically, let f and h be infinitely differentiable smooth curves on a sphere that are parameterized with $\lambda \in [0, 1]$. From these assumptions, we define the perturbation $f + \epsilon g$ shown in Figure 5 as follows:

Definition 1. ϵ -internal division of the geodesic from a to b means a point that contracts by ϵ times along the geodesic from a to b , that is, $\epsilon \cdot d_{Geo}(a, b) = d_{Geo}(a, \epsilon -$

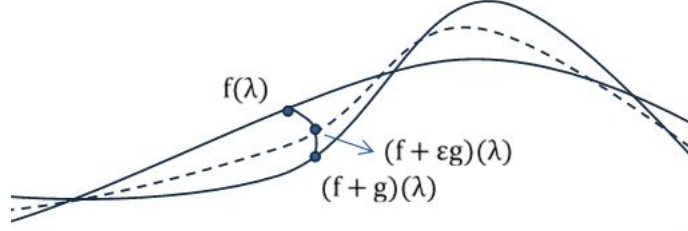


Figure 5: Perturbation of f along geodesic to $f + g$.

internal division).

For $\epsilon < 0$, ϵ -internal division of the geodesic from a to b can be defined in the same manner. We note that when a and b are located on the opposite sides, the shortest geodesic is not unique. Thus, we only consider the case that the distance between $f(\lambda)$ and the perturbation function $(f + g)(\lambda)$ is less than π when the curves are on the unit sphere. It is reasonable since we aim to show the stationarity for small ϵ .

Definition 2. Let f and $f + g$ be smooth curves on a sphere that are parameterized with $\lambda \in [0, 1]$ satisfying $\|g\| := \max_{\lambda \in [0, 1]} d_{Geo}(f(\lambda), (f + g)(\lambda)) \neq \pi$. Then, we define $(f + \epsilon g)(\lambda)$ as ϵ -internal division of the geodesic from $f(\lambda)$ to $(f + g)(\lambda)$ $\forall \lambda \in [0, 1]$.

The following two properties can be obtained from the definition.

Proposition 1. Under the same conditions in Definition 2, $f + \epsilon g$ is a smooth curve on a sphere and $\lim_{\epsilon \rightarrow 0} (f + \epsilon g)(\lambda) = f(\lambda)$ uniformly on $\lambda \in [0, 1]$.

Proof. From the assumption that $f(\lambda)$ and $(f + g)(\lambda)$ are smooth functions and the uniqueness assumption of $(f + \epsilon g)(\lambda)$, the smoothness of $(f + \epsilon g)(\lambda)$ with respect to λ follows. Moreover, it is easy to see that $f + \epsilon g (= f(\epsilon, \lambda))$ is infinitely differentiable on $[-1, 1] \times [0, 1]$. In addition, from the definition of ϵ -internal division and $\|g\| \neq \pi$, the uniform continuity of $(f + \epsilon g)(\lambda)$ on $\lambda \in [0, 1]$ with respect to ϵ follows. \square

In Euclidean space, we have $g(\lambda) = \frac{\partial}{\partial \epsilon} f_\epsilon(\lambda)$, where $f_\epsilon(\lambda) := f + \epsilon g$. From this fact, the magnitude of perturbation $\|h - f\|$ is defined as $g(\epsilon_0, \lambda) := \frac{\partial}{\partial \epsilon} \big|_{\epsilon=\epsilon_0} f_\epsilon(\lambda)$, $\|g(\lambda)\| := d_{Geo}(f(\lambda), g(\lambda)) = |g(\epsilon_0, \lambda)|$, $\|g\| := \max_\lambda \|g(\lambda)\|$, and $\|h - f\| := \|g\| \neq \pi$. The boundedness of $\|g\|$ guarantees that ϵ -internal division of the geodesic from f to h converges to

f uniformly on $\lambda \in [0, 1]$ as ϵ goes to zero. Notice that from the compactness of the unit sphere, $\|h - f\|$ is inherently equal or less than π ; thus, the assumption of $\|h - f\| \neq \pi$ implies that $\|h - f\| < \pi$.

Moreover, the norm of derivative of perturbation $\|(h - f)'\|$ is defined as $g'(\epsilon, \lambda_0) := \frac{\partial}{\partial \lambda} \big|_{\lambda=\lambda_0} g(\epsilon, \lambda)$, $\|g'(\lambda_0)\| := \max_{|\epsilon| \leq 1} \|g'(\epsilon, \lambda_0)\|$, $\|g'\| := \max_{\lambda_0} \|g'(\lambda_0)\|$, and $\|(h - f)'\| := \|g'\|$. It is easy to check that a constraint $\|g'\| \leq 1$ ensures a finite length of $f + \epsilon g$ and well-definedness of $\lambda_{f+\epsilon g}$ for $|\epsilon| \leq 1$. In addition, $(f + \epsilon g)(\lambda)$ is extended to a small open interval containing $[-1, 1]$ for differentiability on $[-1, 1]$.

Let x be a point on a sphere. By the continuity of f and the compactness of the domain set, it follows that $\inf_{\lambda \in [0, 1]} d_{Geo}(x, f(\lambda))$ can be attained. Let $d(x, f)$ denote the geodesic distance between x and f , i.e., $d(x, f) := \min_{\lambda \in [0, 1]} d_{Geo}(x, f(\lambda))$. By the continuity of f again, $\{\lambda \in [0, 1] \mid d_{Geo}(x, f(\lambda)) = d(x, f)\}$ is closed and therefore compact. Thus, the projection index $\lambda_f(x) = \inf\{\lambda \mid d_{Geo}(x, f(\lambda)) = d(x, f)\}$ is well defined. When $\text{card}\{\lambda \mid d_{Geo}(x, f(\lambda)) = d(x, f)\} > 1$, the point x is called an ambiguity point of f . The set of ambiguity points of the smooth curve has spherical measure 0; thus, the ambiguity points are negligible when calculating the expected value.

Let X be a random vector on a sphere that has a probability density. We define that f is an extrinsic principal curve of X when f satisfies the following self-consistency of X ,

$$\pi(E(\xi(X) \mid \lambda_f(X) = \lambda)) = f(\lambda), \text{ for a.e. } \lambda,$$

where ξ denotes the natural embedding from the unit sphere to \mathbb{R}^3 and π is a projection mapping from \mathbb{R}^3 to the sphere, which are used in (4) for the definition of extrinsic mean.

In the principal curve algorithm, it is natural that the projection is made along the geodesic, and therefore, it is reasonable to calculate the distance of (7) as the geodesic distance. However, it is difficult to show that the equation (7) is valid in the spherical surface directly. It seems that the square is a natural operation in the Euclidean space, but not in the spherical surface. Here, by using the spherical law of cosine, we obtain the following result.

Theorem 1. *Suppose that $f, f + g : [0, 1] \rightarrow S^2$ are finite-length smooth curves satisfying $\|g\| \neq \pi$ and $\|g'\| \leq 1$ and X is a random vector on S^2 . Then, f is an extrinsic principal*

curve of X if and only if

$$\left. \frac{dE_X(\cos(d_{Geo}(X, f + \epsilon g)))}{d\epsilon} \right|_{\epsilon=0} = 0. \quad (8)$$

A proof is provided in Appendix. We remark that since $2 - 2\cos x \approx x^2$ for small x , the above result (8) has a similar meaning to (7). Based on this, it is able to consider the sum of $2 - 2\cos(d_{Geo}(x, f))$ in the extrinsic principal curve as the reconstruction error (distance) $\delta(D, f)$. However, $2 - 2\cos(d_{Geo}(x, f))$ is a monotonically increasing function of $d_{Geo}(x, f)$, if $d_{Geo}(x, f) \in [0, \pi]$; hence, there is no difference in which one is used as an evaluation measure or a threshold in the algorithm.

Furthermore, we find a necessary and sufficient condition of intrinsic principal curves on a sphere below.

Theorem 2. *Suppose that $f, f + g : [0, 1] \rightarrow S^2$ are finite-length smooth curves satisfying $\|g\| \neq \pi$ and $\|g'\| \leq 1$ and that a random vector X on S^2 satisfies $X \in B(\zeta)$, where $B(\zeta) := \{x \in S^2 \mid |f''(\lambda_f(x)) \cdot x| > \zeta\}$ for a small $\zeta > 0$. Then, f is an intrinsic principal curve of X if and only if*

$$\left. \frac{dE_X(d_{Geo}^2(X, f + \epsilon g))}{d\epsilon} \right|_{\epsilon=0} = 0. \quad (9)$$

In contrast to the extrinsic stationarity, an additional constraint $X \in B(\zeta)$ is necessary for guaranteeing that the projection index $\lambda_{f_\epsilon}(X)$ is differentiable for ϵ and its derivative is uniformly bounded, which is verified by Lemma 5 in Appendix. Furthermore, the measure of $S^2 \setminus B(\zeta)$ goes to 0 as $\zeta \rightarrow 0$ by Lemma 4 in Appendix. Thus, the constraint of random vector X could be almost negligible by setting ζ infinitesimally small since X has a probability density.

We remark that the stationarity of principal curves in Euclidean space provides a rationale for the principal curves of Hastie and Stuetzle (1998) that is a nonlinear generalization of the linear principal component. Along the same line, the above stationarity results provide theoretical justifications that the proposed approaches extend the principal curves in Euclidean space to the sphere.

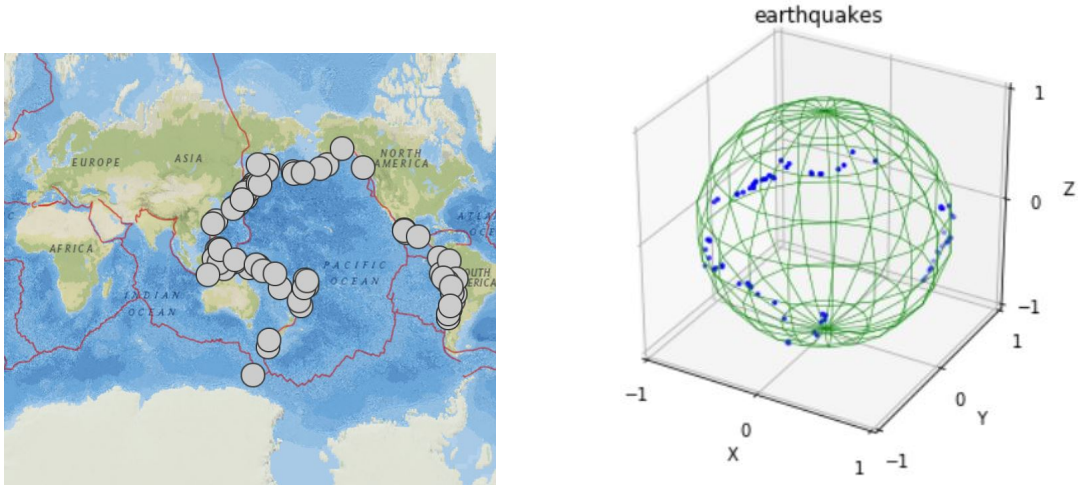


Figure 6: The distribution of significant earthquakes (8+ Mb magnitude), and their three-dimensional visualization.

5 Numerical Experiments

In this section, we conduct numerical experiments with real data analysis and several simulated examples to assess the practical performance of the proposed methods, which are implemented by the algorithms in Section 4. The Python codes used to implement the methods and to carry out some experiments are available at <https://github.com/Janghyun1230/Spherical-Principal-Curve> in order that one can reproduce the same results.

5.1 Real Data Analysis: U.S. Geological Earthquake Survey

Here we present a real data analysis of the proposed principal curves on a sphere. For this purpose, we consider earthquake data from the U.S. Geological Survey in Figure 6 that represent the distribution of significant earthquakes (8+ Mb magnitude) around the Pacific Ocean since the year 1900. As shown in Figure 6, we observe some features of the data: (a) the observations are scattered on the surface of Earth, and (b) they are non-linear one-dimensional structure on the sphere. It seems that the proposed principal curve might be applicable to the data for extracting the feature.

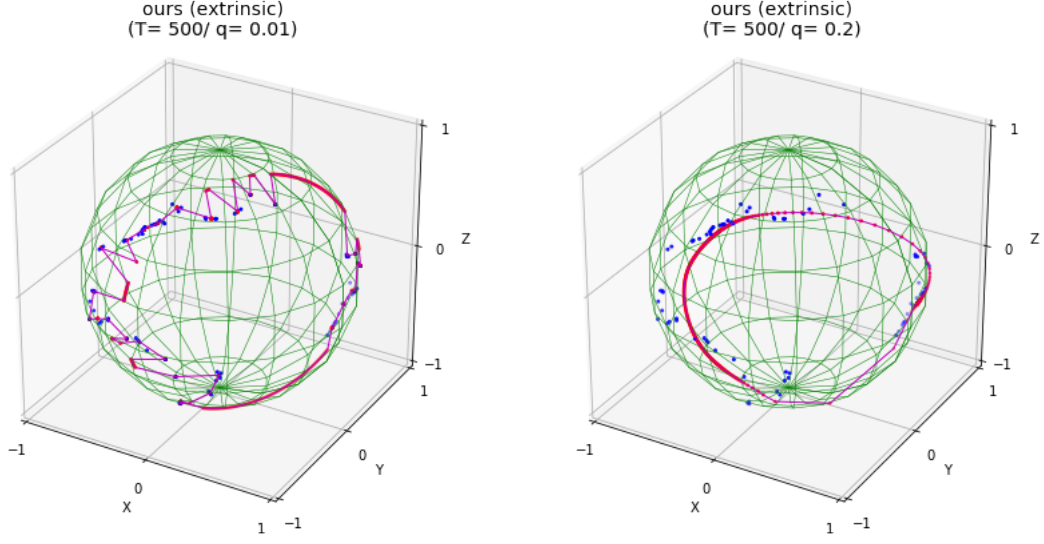


Figure 7: Principal curves (extrinsic) of $T = 500$ points with $q = 0.01$ (left) and $q = 0.2$ (right). Blue points represent the earthquake data and red points represent the points of the fitted curve.

We now perform the proposed extrinsic principal curve over different values of hyperparameter q . As q decreases, the resulting curve becomes wiggly and overfits the data. Figure 7 shows the results with $q = 0.01$ and 0.2 . The determination of the parameter q is not easy. Duchamp and Stuetzle (1996) showed that a principal curve is always a saddle point of the expected squared distance function, which explains why cross-validation is not reliable for choosing hyperparameter q . In Euclidean space, Biau and Fischer (2012) suggested the parameter selection by empirical risk minimization via penalization of length and the number of points in curves. In a spherical domain, this topic is left for future work. As mentioned earlier, the proposed algorithm is required to have an initialization. The results in Figure 7 are obtained by using $T = 500$ uniformly sampled points from the intrinsic principal circle in Section 3.2 as an initialization.

We further compare the proposed extrinsic principal curves with the principal curves of Hauberg (2016). Figure 8 shows both results with $q = 0.1$, where the purple lines represent the fitted curves by each method, and the blue lines represent the projections from the data onto the curve. As one can see, the proposed extrinsic principal curve continuously

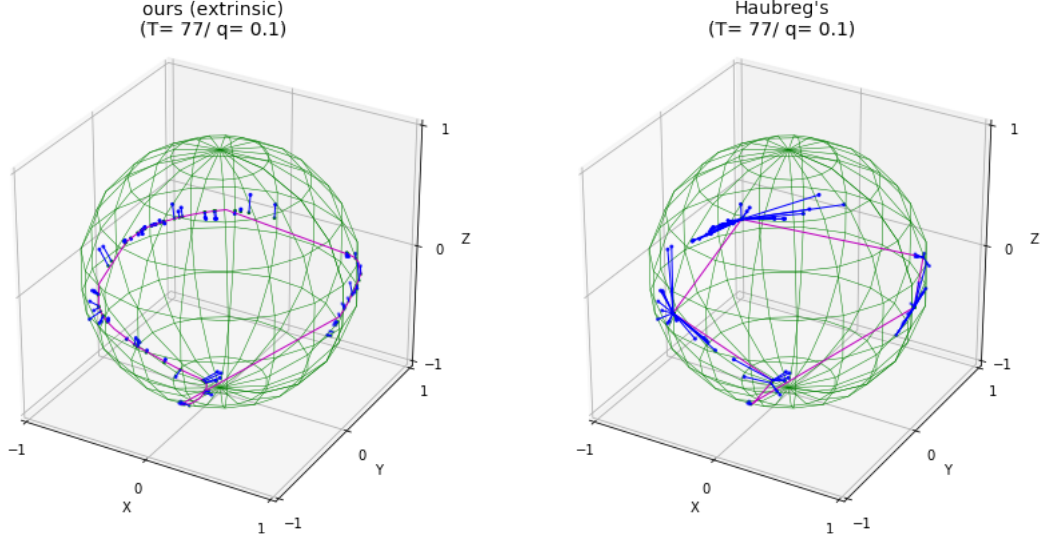


Figure 8: Projection results by the proposed method (left) and Hauberg’s method (right), $T = 77$ and $q = 0.1$.

represents the given data on the curve, whereas the principal curve of Hauberg (2016) projects some local data points to a single point. The results are further summarized in Table 1. When 77 earthquake observations are projected on the principal curve, the number of distinct projections by our method is much larger than that of Hauberg’s method. It implies that our principal curve represents the data continuously, compared to Hauberg’s principal curve that tends to cluster the data. Moreover, through a reconstruction error defined as $\sum_{i=1}^n d_{Geo}^2(x_i, \hat{f}(\lambda_{\hat{f}}(x_i)))$ with the observations x_i and fitted values $\hat{f}(\lambda_{\hat{f}}(x_i))$, we compare both methods and observe that our method outperforms Hauberg’s method.

5.2 Simulation Study

To evaluate the empirical performance of the proposed method, we conduct a simulation study. For this purpose, we consider two types of form on the unit sphere with spherical coordinates $(r = 1, \theta, \phi)$, where θ is the azimuthal angle, and ϕ denotes polar angle.

- Circle: It is formed of $(r = 1, \theta, \phi)$ with $0 \leq \theta < 2\pi$ and $\phi = \pi/4$. It is an ideal case for the extrinsic principal curve as well as the improved principal circle.
- Wave: It is defined as $(r = 1, \theta, \phi)$ with $0 \leq \theta < 2\pi$ and $\phi = \alpha \sin(2\pi\theta f) + \pi/2$. It has

Table 1: Comparison of extrinsic principal curve and Hauberg’s.

			extrinsic	intrinsic	Hauberg
T=77	q=0.2	Reconstruction error	2.662	4.391	12.067
		# of distinct projection	74/77	72/77	22/77
	q=0.1	Reconstruction error	0.463	0.467	4.920
		# of distinct projection	76/77	76/77	9/77
	q=0.05	Reconstruction error	0.359	0.359	1.313
		# of distinct projection	74/77	73/77	16/77
	q=0.01	Reconstruction error	0.061	0.061	0.227
		# of distinct projection	75/77	75/77	27/77
T=500	q=0.2	Reconstruction error	2.193	3.460	11.300
		# of distinct projection	75/77	72/77	30/77
	q=0.1	Reconstruction error	0.715	0.732	3.903
		# of distinct projection	75/77	74/77	18/77
	q=0.05	Reconstruction error	0.298	0.200	0.963
		# of distinct projection	75/77	75/77	27/77
	q=0.01	Reconstruction error	0.036	0.036	0.121
		# of distinct projection	75/77	75/77	37/77

a complicated structure with varying frequency ($f = 4, 8$) or amplitude of waveform ($\alpha = 1/3, 1/6$).

For each dataset, we generate $n = 100$ data points from each form by sampling θ equally in $[0, 2\pi]$, and add normal noises from $N(0, \sigma^2)$ on ϕ with a certain noise level σ . Figure 9 shows a realization of noisy circular data with $\sigma = 0.07$ marked by blue and the extrinsic principal curve by the proposed method with $T = 500$ and $q = 0.05$ that represents the underlying structure well.

We now consider a dataset with the wave structure, in which the principal circle cannot reveal the wave feature, while the proposed principal curve might be capable of extracting the feature. To conduct various experiments, we use several forms of wave, parameterized by amplitude $\alpha = 1/6, 1/3$ and frequency $f = 4, 8$. In addition, a sampling rate of the data point is considered for the experiment setting.

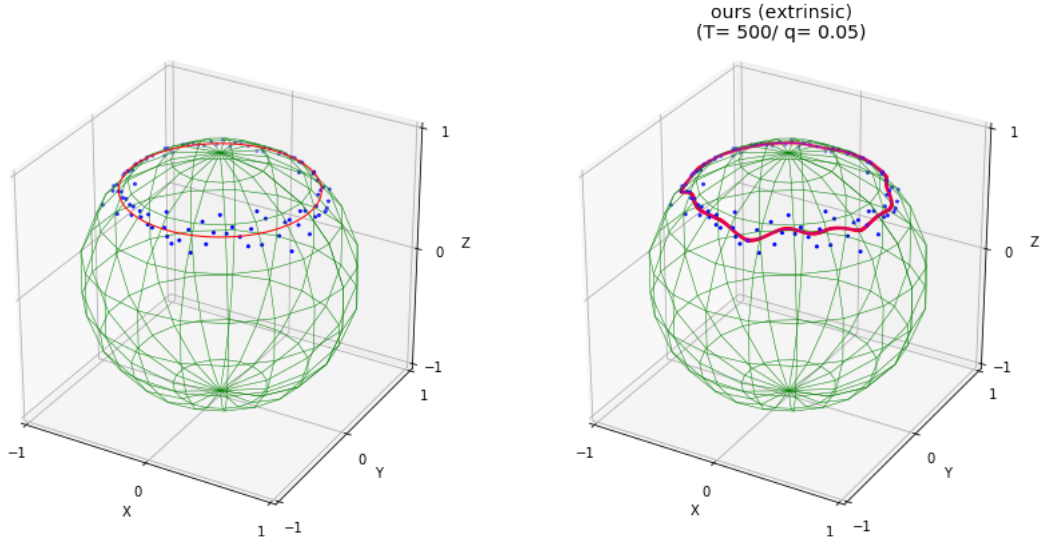


Figure 9: True circular curve and blue noisy data (left), and the extrinsic principal curve with $T = 500$ and $q = 0.05$ (right).

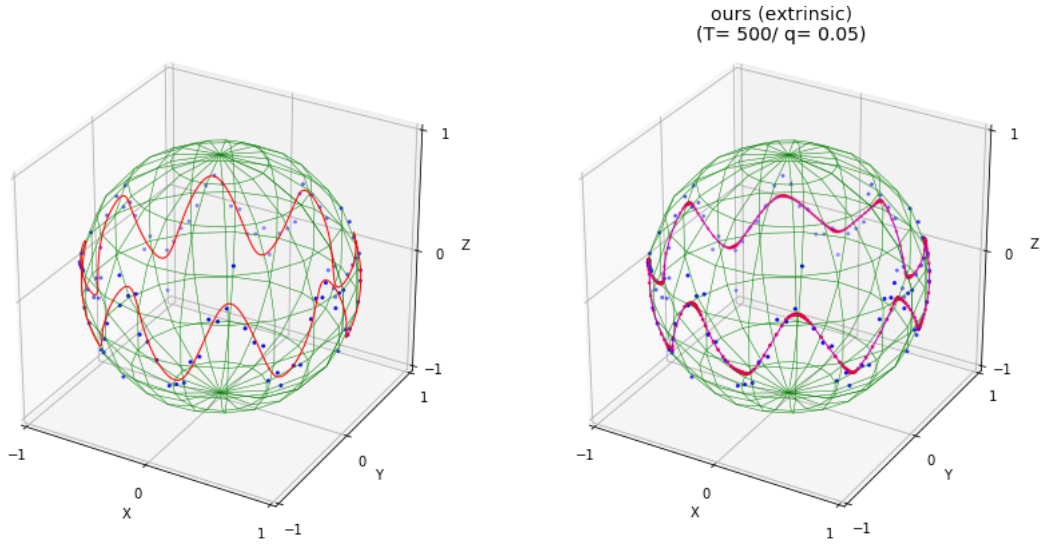


Figure 10: True waveform curve and blue noisy data (left), and the extrinsic principal curve with $T = 500$ and $q = 0.05$ (right).

Firstly, a waveform dataset with the amplitude of $\alpha = 1/3$ and the frequency of $f = 8$ is generated. Figure 10 shows the underlying structure, noisy data, and the extrinsic principal curve with $T = 500$ and $q = 0.05$ that represents the underlying waveform efficiently. Notice that the amplitude of principal curves is reduced owing to the locally weighted averaging in the expectation step of the algorithms when segments of the underlying structure have high curvature, which is a general phenomenon of the original principal curves (Banfield and Raftery, 1992). Secondly, we consider a waveform dataset with amplitude $\alpha = 1/3$ and relatively low frequency $f = 4$ in Figure 11. We compare our methods with Hauberg’s method under the same condition $T = 500$ and $q = 0.05$. As one can see, both extrinsic and intrinsic principal curves extract the true waveform effectively, while Hauberg’s method yields rather a sharp curve. Thirdly, Figure 12 shows a noisy waveform dataset with relatively low amplitude $\alpha = 1/6$ and frequency $f = 8$ and the true waveform. The result by the proposed method represents the waveform feature well, as shown in the right panel. Lastly, in Figure 13, we use a waveform with high amplitude $\alpha = 1/3$ and high frequency $f = 8$ as the first case, but take a low sampling rate that the number of data points is small, $n = 50$, compared to the case of Figure 10. In other words, the generated data are rather sparse. The result by the proposed method in the right panel produces a sawtooth form, but it still represents the up-down pattern roughly on the sphere.

For further evaluation, we conduct a Monte Carlo simulation. For this purpose, we generate noisy data that consist of two true curves and Gaussian noises from $N(0, \sigma^2)$ with a noise level of $\sigma = 0.07$ or 0.1 . The number of data points is $n = 100$, and data points are equally spaced. We consider three methods for feature extraction, the proposed extrinsic, intrinsic principal curves, and the principal curve by Hauberg (2016). As an evaluation measure, we consider a reconstruction error defined as $\sum_{i=1}^n d_{Geo}^2(x_i, \hat{f}(\lambda_{\hat{f}}(x_i)))$, where x_i denote sample values of the true function and $\hat{f}(\lambda_{\hat{f}}(x_i))$ are the fitted values. In addition, we use the number of distinct projection points as another evaluation measure. It can be conjectured that the resulting curve with a large number of distinct projection points represents data continuously.

For each combination of the underlying curve and noise level, we generate equally spaced data points with size $n = 100$ and then compute the reconstruction error and

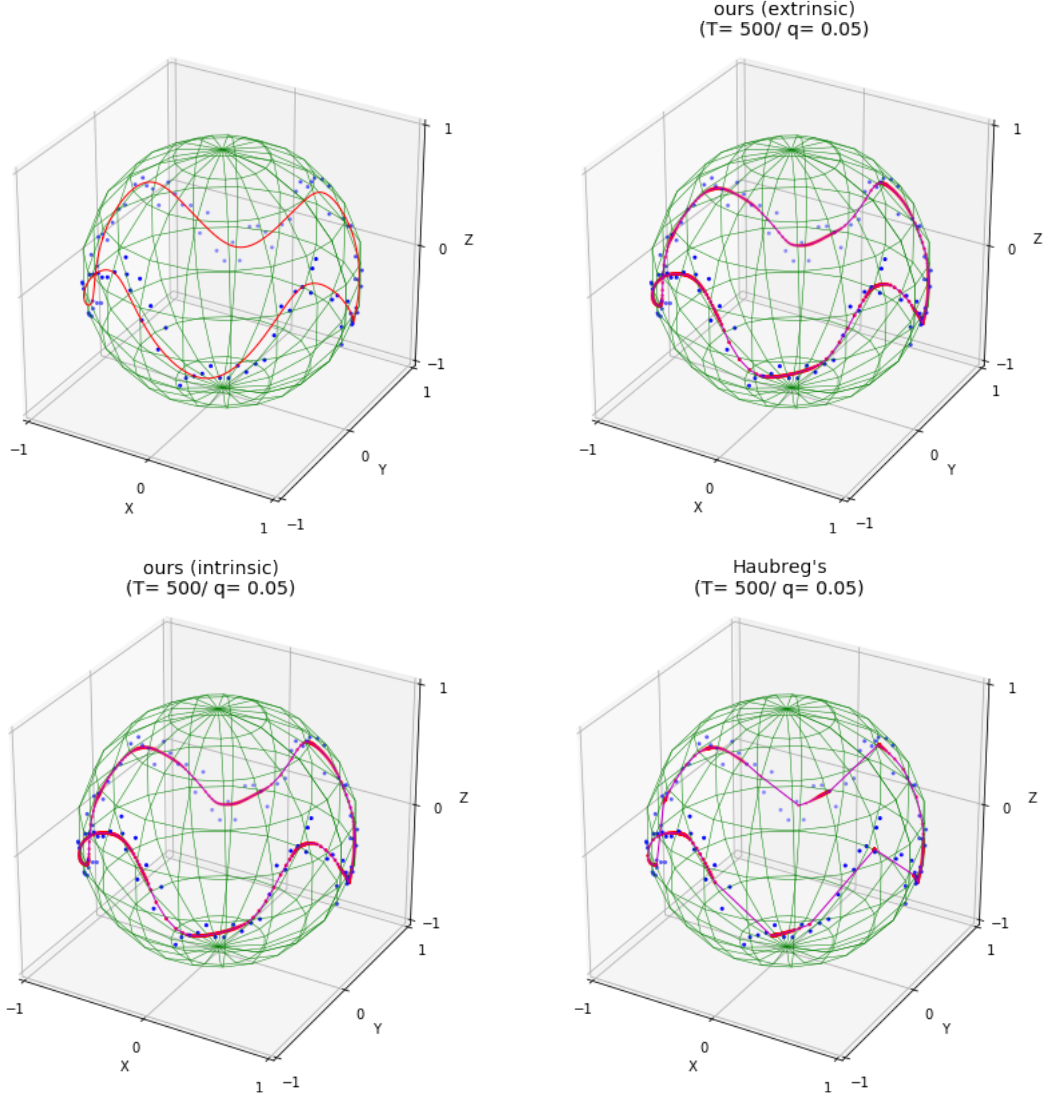


Figure 11: From left to right and top to bottom: True waveform and noisy data, the extrinsic principal curve, the intrinsic principal curve, and the curve by Hauberg’s method.

the number of distinct projection points by each method. Over 50 simulation data sets, Table 2 lists the average values of reconstruction errors and their standard deviations. As listed, the proposed principal curves outperform the method of Hauberg (2016). Table 3 provides average values of distinct projection points and their standard deviations. As one can see, the proposed method provides a much large number of distinct projection points, compared to that of Hauberg (2016). Overall, as listed in Tables 2 and 3, the proposed

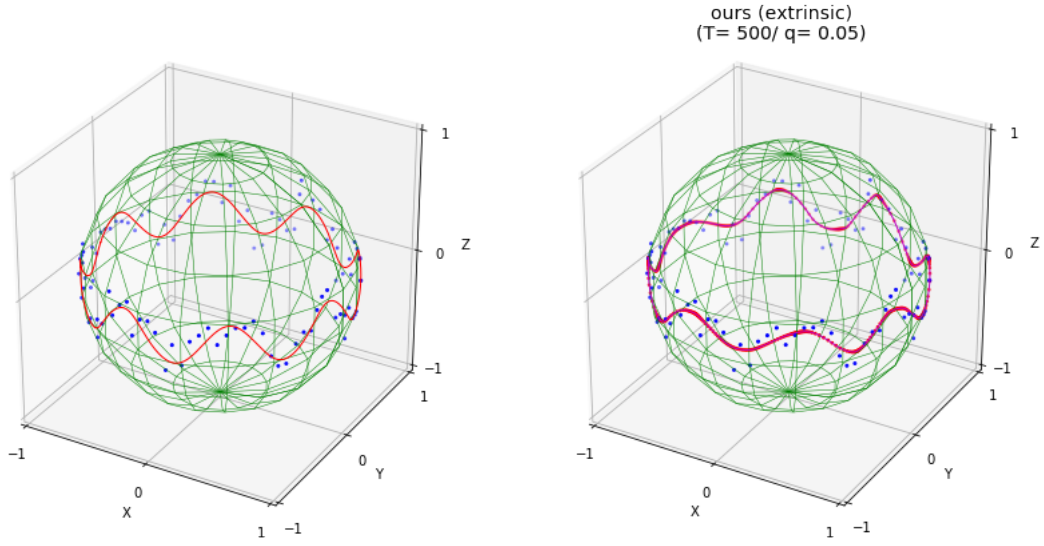


Figure 12: True waveform of low amplitude and noisy data (left), and the extrinsic principal curve with $T = 500$ and $q = 0.05$ (right).

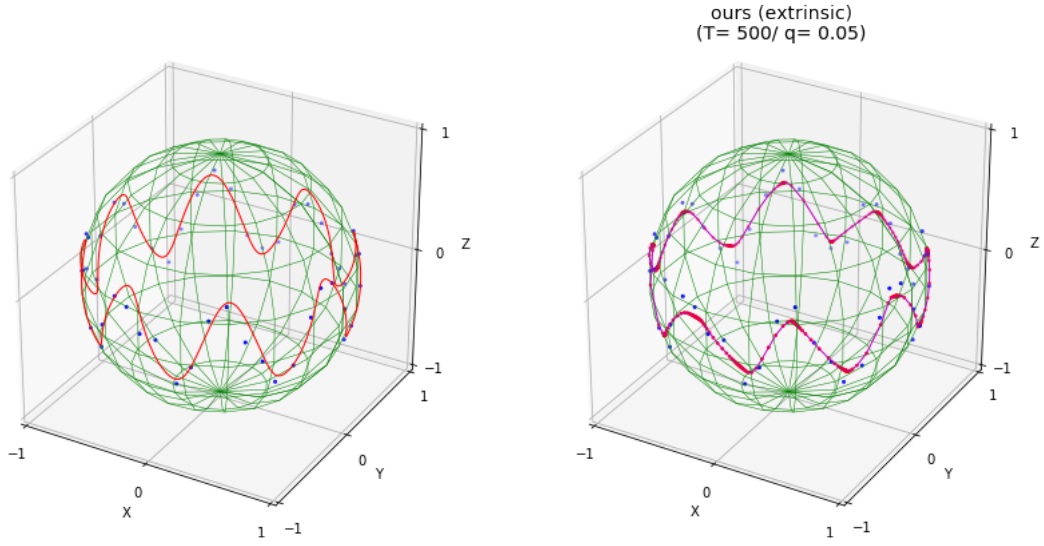


Figure 13: True waveform and a sparse dataset with 50 data points (left), and the extrinsic principal curve with $T = 500$ and $q = 0.05$ (right).

Table 2: Averages of reconstruction errors and their standard deviations in the parentheses by each method.

	True form	Method	Noise level					
			$\sigma = 0.07$			$\sigma = 0.1$		
			$q = 0.05$	$q = 0.03$	$q = 0.01$	$q = 0.05$	$q = 0.03$	$q = 0.01$
$T = 100$	Circle	Proposed(extrinsic)	0.093 (0.026)	0.12 (0.026)	0.095 (0.013)	0.201 (0.049)	0.218 (0.042)	0.138 (0.025)
		Proposed(intrinsic)	0.093 (0.026)	0.12 (0.027)	0.095 (0.013)	0.201 (0.048)	0.216 (0.046)	0.137 (0.025)
		Hauberg	0.117 (0.073)	0.408 (0.149)	0.298 (0.038)	0.370 (0.205)	0.74 (0.208)	0.494 (0.063)
	Wave	Proposed(extrinsic)	0.703 (0.116)	0.338 (0.092)	0.084 (0.026)	0.679 (0.136)	0.353 (0.108)	0.124 (0.037)
		Proposed(intrinsic)	0.71 (0.114)	0.329 (0.097)	0.084 (0.023)	0.673 (0.150)	0.346 (0.113)	0.124 (0.038)
		Hauberg	2.444 (0.059)	2.158 (0.155)	0.568 (0.055)	2.544 (0.118)	2.103 (0.563)	0.796 (0.094)
$T = 500$	Circle	Proposed(extrinsic)	0.088 (0.026)	0.118 (0.023)	0.091 (0.018)	0.209 (0.049)	0.212 (0.043)	0.129 (0.018)
		Proposed(intrinsic)	0.088 (0.026)	0.118 (0.023)	0.091 (0.018)	0.21 (0.050)	0.207 (0.043)	0.129 (0.018)
		Hauberg	0.089 (0.027)	0.205 (0.079)	0.269 (0.034)	0.233 (0.087)	0.453 (0.177)	0.397 (0.079)
	Wave	Proposed(extrinsic)	0.531 (0.064)	0.239 (0.058)	0.072 (0.020)	0.57 (0.094)	0.237 (0.081)	0.110 (0.031)
		Proposed(intrinsic)	0.535 (0.065)	0.239 (0.056)	0.072 (0.020)	0.574 (0.094)	0.237 (0.082)	0.110 (0.031)
		Hauberg	2.006 (0.697)	1.831 (0.146)	0.529 (0.043)	1.906 (0.847)	1.756 (0.696)	0.688 (0.073)

methods perform better than Hauberg’s method, including the case that $T = 500$ is much larger than $n = 100$ in which Hauberg’s method is improved. In addition, the results of both intrinsic and extrinsic principal curves are similar in terms of reconstruction error and the number of distinct projection points, which is along with the fact that the intrinsic and extrinsic means are almost identical in the local region (Bhattacharya and Patrangenaru, 2005).

6 Median Principal Curves: A Robust Extension

The intrinsic mean is obtained by the minimization of the sum of square of the geodesic distances; thus, the intrinsic principal curves might be sensitive to outliers. By following the conventional way in Euclidean space, it is natural to consider the median as an alternative measure of the centrality of data. In particular, we replace the expectation step in Algorithm 3 with

$$C_t = \arg \min_x \sum_i w_{t,i} \cdot d_{Geo}(x, x_i), \quad t = 1, \dots, T.$$

Table 3: Averages of distinct projection points and their standard deviations in the parentheses by each method.

	True form	Method	Noise level					
			$\sigma = 0.07$			$\sigma = 0.1$		
			$q = 0.05$	$q = 0.03$	$q = 0.01$	$q = 0.05$	$q = 0.03$	$q = 0.01$
$T = 100$	Circle	proposed(extrinsic)	99.06 (0.31)	98.96 (0.40)	98.80 (0.45)	99.06 (0.31)	98.6 (1.12)	98.10 (1.05)
		proposed(intrinsic)	99.02 (0.32)	98.92 (0.34)	98.84 (0.47)	99.08 (0.34)	98.72 (1.11)	98.20 (1.12)
		Hauberg	87.70 (7.95)	56.68 (17.99)	64.70 (3.22)	69.80 (12.28)	47.04 (15.44)	60.42 (2.83)
	Wave	proposed(extrinsic)	93.36 (4.50)	96.88 (1.96)	99.30 (0.54)	94.98 (3.86)	96.36 (2.34)	99.00 (0.67)
		proposed(intrinsic)	93.36 (4.47)	97.28 (2.13)	99.32 (0.51)	95.82 (3.77)	96.72 (2.22)	99.10 (0.65)
		Hauberg	22.72 (2.77)	25.94 (2.65)	62.14 (2.49)	24.5 (3.63)	32.16 (16.72)	58.84 (3.04)
$T = 500$	Circle	proposed(extrinsic)	99.06 (0.24)	99.08 (0.40)	98.72 (0.58)	99.08 (0.27)	98.94 (0.47)	98.14 (1.03)
		proposed(intrinsic)	99.08 (0.27)	99.02 (0.25)	98.76 (0.69)	99.1 (0.30)	99.04 (0.49)	99.30 (1.09)
		Hauberg	97.8 (1.47)	89 (8.63)	79.28 (4.60)	93.64 (5.29)	78.72 (13.08)	73.86 (7.28)
	Wave	proposed(extrinsic)	99.16 (0.37)	98.5 (1.40)	99.28 (0.64)	99.18 (0.39)	98.68 (1.22)	99.30 (0.74)
		proposed(intrinsic)	99.18 (0.39)	98.5 (1.27)	99.26 (0.56)	99.22 (0.42)	98.84 (1.20)	99.18 (0.66)
		Hauberg	45.2 (24.8)	43.38 (3.72)	73.20 (3.42)	52.04 (26.81)	50.64 (19.99)	71.52 (4.38)

Then the resulting curves pass through the “median” of the given dataset. We now define a median principal curve, by mimicking the principal curve of (1), as

$$f(\lambda) = \text{Median}[X | \lambda_f(X) = \lambda] \text{ for a.e. } \lambda,$$

where the points projecting onto $f(\lambda)$ are contained in a set of a great circle on the sphere, $M_\lambda := \{x \in S^2 : \lambda_f(x) = \lambda\}$, and a connected proper subset of M_λ is isometric to a line with the same length in \mathbb{R} . Thus, the above-median can be found in the same way in \mathbb{R} . More specifically, for a given dataset $\{x_1, x_2, \dots, x_n\} \subset S^2$, the point on the sphere that minimizes the function $f(x) := \frac{1}{n} \sum_{i=1}^n d_{Geo}(x, x_i)$ is called *geometric median*, which has no explicit form (Bajaj, 1988). Thus, it should be obtained by a numerical algorithm. By a similar way in Buss and Fillmore (2001), we have

$$\nabla f(x) = -\frac{1}{n} \sum_{i=1}^n \log_x(x_i) / \|\log_x(x_i)\|$$

for $x \notin \{x_1, x_2, \dots, x_n\}$. Here is a practical algorithm for finding geometric median on a sphere by gradient descent.

Algorithm 4 Geometric Median on Sphere

For given data $x_1, \dots, x_n \in S^2$ and their weights $w_1, \dots, w_n \geq 0$ such that $\sum_{i=1}^n w_i > 0$, select initial geometric median as $M_1 = x_1$.

while ($\Delta M \geq \text{threshold}$) **do**

- $\Delta M = \frac{1}{j} \cdot \sum_{1 \leq i \leq n, x_i \neq M_j} \frac{w_i}{\sum_{i=1}^n w_i} \cdot \log_{M_j}(x_i) / \|\log_{M_j}(x_i)\|.$
- $M_{j+1} = \exp_{M_j}(\Delta M).$

end while

In the case that a dataset on the unit sphere is contained in a convex region U in which any geodesic distance between two points in U is less than $\frac{\pi}{2}$, the geometric median exists and is unique (Fletcher et al., 2009). In practice, it is necessary to obtain the geometric median only on a small region in the expectation step of the principal curve algorithm, say Algorithm 3. Meanwhile, notice that we divide a gradient part by iteration j to get ΔM for each iteration. In contrast to the intrinsic mean, ΔM is a weighted average of the unit vectors; thus, it is possible that its length does not go to 0, and the algorithm could oscillate and not converge. Heuristically, to cope with this problem, we divide it by the number of iterations j , so the length of ΔM goes to 0 as $j \rightarrow \infty$. Moreover, it is able to reach the goal finally because of $\sum_{j \in \mathbb{N}} \frac{1}{j} = \infty$. Algorithm 4 works and is empirically stable. To reduce the computational cost, the denominator could be considered as j^α ($0 < \alpha < 1$) instead of j .

Furthermore, we investigate the stationarity of the median principal curves as follows.

Theorem 3. *Under the same conditions on Theorem 2, f is a median principal curve of X if and only if*

$$\left. \frac{dE_X(d_{Geo}(X, f + \epsilon g))}{d\epsilon} \right|_{\epsilon=0} = 0. \quad (10)$$

We now present a simulated example for the empirical performance of the proposed median principal curves. For this purpose, we consider the circular data on the sphere, which is formed of $(r = 1, \theta, \phi)$ with $0 \leq \theta < 2\pi$ and $\phi = \pi/4$. We generate $n = 200$ data points by sampling θ equally in $[0, 2\pi]$, and add random noises from $\text{Cauchy}(0, 0.05)$ on ϕ . As shown in Figure 14, the median principal curve implemented with $T = 100$ and

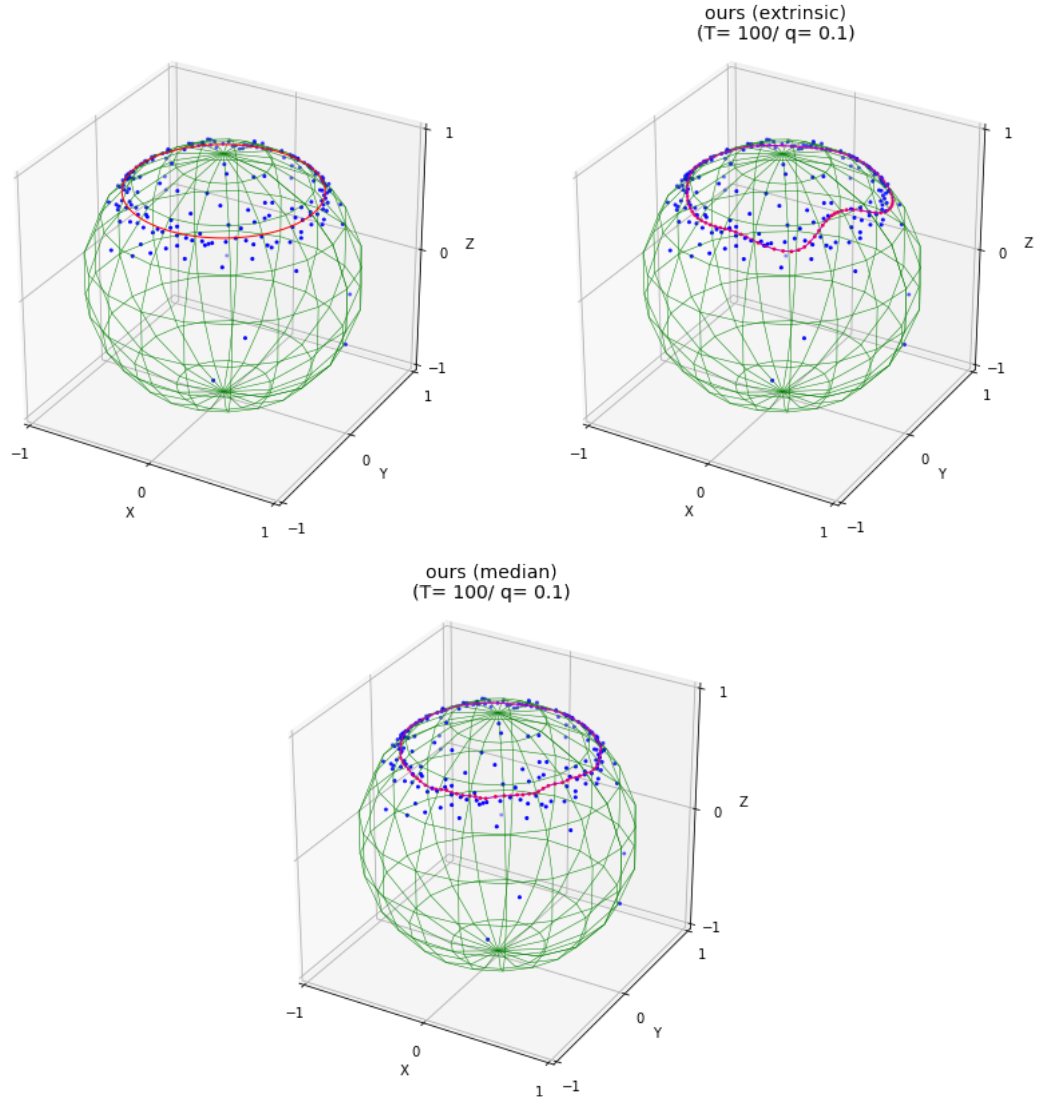


Figure 14: True circular curve and noisy data (left), the extrinsic principal curve with $T = 100$ and $q = 0.1$ (right), and the median principal curve with $T = 100$ and $q = 0.1$ (bottom).

$q = 0.1$ is robust to the outliers and represents the underlying structure well, compared to the extrinsic principal curve.

7 Concluding Remarks

In this paper, we have proposed new principal curves on a sphere for dimension reduction of spherical data. For this purpose, we have considered the extrinsic and intrinsic approaches and investigated the stationarity of the principal curves which supports that the proposed methods are a direct extension of principal curves (Hastie and Stuetzle, 1989) to a sphere.

As far as Euclidean space is concerned as embedding space, dimension, or location of the origin does not affect the distance, and hence, does not affect the extrinsic mean. Moreover, the extrinsic approach holds efficiency computationally. However, it is questionable whether an extrinsic approach is still effective in asymmetric manifolds. For some asymmetric manifolds, an intrinsic approach may yield better performance. Moreover, the intrinsic mean defined by a given geodesic distance might be attractive owing to its inherency. However, the iterative way for the intrinsic mean is computationally expensive since it takes time for the algorithm to converge.

In this study, the proposed principal curve algorithm is a top-down approach, in the sense that it approximates the structure of data as an initial curve and then improve the approximation gradually in an iterative manner. Thus, initialization plays a crucial role in the algorithm. The intrinsic principal circle in Section 3.2 has been used as the initialization of the proposed principal curve. It is capable of identifying some meaningful structure of spherical data. However, there exist some complex structures that cannot be represented only by a circle, for example, a structure divided into several pieces or a structure with intersections. To cope with this limitation, it is worth to study a “bottom-up” approach, which is left for future work.

As final remarks, in shape analysis or motion analysis, data have been represented as a Cartesian product of \mathbb{R} , \mathbb{R}^+ and $\text{SO}(2)$. PGA by Fletcher et al. (2004) and the principal arc analysis by Jung et al. (2011) perform dimension reduction on medial representation by mapping the given data space to Euclidean space. If the data are properly projected on geodesic segments, the proposed principal curve procedure can be applied for medial representation. Since the mean can be independently calculated for each component of the Cartesian product, there is no additional difficulty in the expectation step. Some problems

of projecting from the Cartesian product of simple manifolds to geodesic segments are left for future study.

Appendix: Stationarity of Principal Curves

Throughout this discussion, we cover finite-length smooth curve that does not cross on a sphere (i.e., $\lambda_1 \neq \lambda_2 \in [0, 1] \Rightarrow f(\lambda_1) \neq f(\lambda_2)$), including curves with end points as well as closed curves, which can be both parameterized by the closed interval $[0, 1]$. In the latter case, boundary condition is needed; any order partial derivatives of f at 0 and 1 are the same, i.e., $f^{(k)}(0) = f^{(k)}(1)$ for all $k \geq 0$. For a random vector X on a sphere, we further assume that the curve f is not short enough to cover X well, that is, $\lambda_f(X) \in (0, 1)$ for a.e. X , which implies that X is orthogonally projected on the curve f . Note that f is infinitely differentiable on $[0, 1]$, i.e., f is smoothly extended to open interval containing $[0, 1]$ and all the its derivatives on $[0, 1]$ are continuous. Our main purpose is to prove the stationarity of extrinsic, intrinsic, and median principal curves $f : [0, 1] \rightarrow S^2$ that satisfies the equations (8), (9), and (10) in Theorems 1, 2, and 3.

When moving from Euclidean space to spherical surface, topological properties such as measurability and continuity are preserved, while the formula using specific distance should be modified. This modification could be obtained by embedding a spherical surface into a three-dimensional Euclidean space. Specifically, we embed a spherical surface as a unit sphere centered at the origin and investigate further derivations. For a smooth curve $f : [0, 1] \rightarrow S^2$, suppose that f is parameterized by a constant speed with respect to λ and is expressed as three-dimensional coordinates $(f(\lambda)_1, f(\lambda)_2, f(\lambda)_3)$. Then the following lemmas are held.

Lemma 1. *The curve f satisfies $f'(\lambda) \cdot f(\lambda) = 0$ and $f''(\lambda) \cdot f'(\lambda) = 0$, $\forall \lambda \in [0, 1]$, where \cdot denotes inner product in \mathbb{R}^3 .*

Proof. It is directly obtained from $f(\lambda) \cdot f(\lambda) = 1$ and $f'(\lambda) \cdot f'(\lambda) = \text{constant}$. □

Lemma 2. *Suppose that $f(\lambda)$ and x are expressed as three-dimensional vectors. Then, it follows that $d_{Geo}(f(\lambda), x) = \arccos(f(\lambda) \cdot x)$, where $\arccos(f(\lambda) \cdot x)$ is the angle be-*

tween $f(\lambda)$ and x . Then, $\frac{df}{d\lambda}(\lambda_f(0,0,1))_3 = 0$. Thus, it follows that $\frac{df}{d\lambda}(\lambda_f(0,0,1)) = a(-f(\lambda_f(0,0,1))_2, f(\lambda_f(0,0,1))_1, 0)$ for some $a \in \mathbb{R}$. Note that $\lambda_f(x)$ denotes the projection index of point x to the curve f .

Proof. For $p = (0, 0, 1)$, it follows that $d_{Geo}(f(\lambda), p) = \arccos(f(\lambda)_3)$. From the assumption that $f(\lambda)$ is a smooth curve and the fact that $d_{Geo}(f(\lambda), p)$ has the minimum at $\lambda_f(0, 0, 1)$, the remaining part of the lemma follows by differentiation with respect to λ . \square

Lemma 3. (*Spherical law of cosines*) Let u, v, w be points on a sphere, and a, b and c denote $d_{Geo}(w, u)$, $d_{Geo}(w, v)$ and $d_{Geo}(u, v)$, respectively. If C is the angle between a and b , i.e., the angle of the corner opposite c , then, $\cos c = \cos a \cos b + \sin a \sin b \cos C$. Further, with three-dimensional vectors u, v, w , it follows that $\sin a \sin b \cos C = (w \times u) \cdot (w \times v)$, where \times denotes outer product in \mathbb{R}^3 .

The next topological properties of the principal curves established in Euclidean space of Hastie and Stuetzle (1989) are still valid in spherical surfaces.

Proposition 2. (*Measurability of index function*) For a continuous curve f on a sphere, $\lambda_f(x)$ is measurable.

Proposition 3. (*Continuity of projection index under perturbation*) If x is not an ambiguity point for continuous curve f , then $\lim_{\epsilon \rightarrow 0} \lambda_{f+\epsilon g}(x) = \lambda_f(x)$.

In the proof of Proposition 3, we use the triangle inequality on a sphere. Moreover, by the smoothness and compact domain of f ; $[0, 1]$, we have a more efficient tool for verifying Theorem 2 and 3.

Proposition 4. (*Uniform continuity of projection index under perturbation*) $\lim_{\epsilon \rightarrow 0} \lambda_{f+\epsilon g}(x) = \lambda_f(x)$ uniformly on the set of non-ambiguity points of f . That is, for every $\eta > 0$, there exists $\delta > 0$ such that for any non-ambiguity points x , if $|\epsilon| < \delta$, then $|\lambda_{f_\epsilon}(x) - \lambda_f(x)| < \eta$.

For guaranteeing uniform continuity of projection index, it is required that $|f''|$ is bounded. A proof is similar to that of Proposition 3; thus, we omit the proof, which can be provided on request.

Proposition 5. *Spherical measure of the set of ambiguity points of smooth curve f is 0.*

Detailed steps for a proof of Proposition 5 are similar with those of Hastie and Stuetzle (1989); thus, we omit the proof, which can be provided on request.

Meanwhile, to prove Theorem 2 and 3, it is crucial to verify that λ_{f_ϵ} is differentiable for ϵ and its derivative is uniformly bounded. Thus, it is necessary to define a subset of S^2 as $B(\zeta) := \{x \in S^2 \mid |f''(\lambda_f(x)) \cdot x| > \zeta\}$ for $\zeta \geq 0$. Note that $B(\zeta)$ is increasing as ζ goes to 0 by definition.

Lemma 4. *The image of smooth function from $[0, 1]$ to S^2 has measure 0. Moreover,*

$$S^2 \setminus B(0) = \{x \in S^2 \mid |f''(\lambda_f(x)) \cdot x| = 0\}$$

is a union of images of two smooth functions from $[0, 1]$ to S^2 , which implies that $S^2 \setminus B(0)$ are measure 0. Therefore, the measure of $S^2 \setminus B(\zeta)$ goes to 0 as $\zeta \rightarrow 0$.

Proof. Suppose that I is a smooth function on the sphere, that is, $I : [0, 1] \rightarrow S^2$. The domain and range are the second countable differentiable manifolds whose dimensions are 1 and 2, respectively. Since f is twice continuously differentiable function and the differential dI has rank 1 which is less than dimension of S^2 , by Sard's Theorem, the image $I([0, 1]) = \{I(x) \in S^2 \mid x \in [0, 1]\}$ has measure zero. Next, each point of $S^2 \setminus B(0)$ is characterized by two equations $f'(\lambda) \cdot x = 0$ and $f''(\lambda) \cdot x = 0$ for some $\lambda \in [0, 1]$. Therefore, we define functions I_1, I_2 as follows: For all $\lambda \in [0, 1]$,

$$I_1(\lambda) = f'(\lambda) \times f''(\lambda) / \|f'(\lambda) \times f''(\lambda)\|, \quad I_2(\lambda) = -f'(\lambda) \times f''(\lambda) / \|f'(\lambda) \times f''(\lambda)\|,$$

It is well known that the curvature of a smooth curve lying on the unit sphere is more than 1. It implies that $\kappa = \frac{|f''|}{s^2} \geq 1$, where κ is the curvature of f and $s := |f'(\lambda)| > 0$ for all $\lambda \in [0, 1]$, and hence $f'' \neq 0$. We have already known that $f' \cdot f'' = 0$ by Lemma 1. Hence, it is obtained that $f' \times f'' \neq 0$, which means that I_1 and I_2 are well defined and smooth functions. Therefore, we have $S^2 \setminus B(0) = I_1([0, 1]) \cup I_2([0, 1])$, which completes the proof. \square

Lemma 4 implies that the constraints of random vector X in Theorems 2 and 3 are almost negligible by setting ζ infinitesimally small. It is also used for verifying Theorem 3. Denote the set of ambiguity points of smooth curve f on a sphere as A , which is a measure zero set by Proposition 5.

Lemma 5. *Let A be the set of non-ambiguity points of smooth curve f on a sphere. Suppose that $x \in A \cap B(\zeta)$ for some small $\zeta > 0$, and $\lambda_f(x) \in (0, 1)$. Then $\lambda(\epsilon) := \lambda_{f_\epsilon}(x)$ is a smooth function for ϵ on an open interval containing zero. Moreover, $\frac{\partial \lambda(\epsilon)}{\partial \epsilon}$ is uniformly bounded on $A \cap B(\zeta)$. That is, there exists a constant $C > 0$ and $\delta > 0$ such that if $|\epsilon_0| < \delta$ and $x \in A \cap B(\zeta)$, then $\left| \frac{\partial \lambda_{f_\epsilon}(x)}{\partial \epsilon} \Big|_{\epsilon=\epsilon_0} \right| < C$.*

Proof. Since x is a non-ambiguity point of f and $\lambda_f(x) \in (0, 1)$, $\lambda(\epsilon)$ is uniquely characterized by orthogonality between geodesic from x to $f_\epsilon(\lambda(\epsilon))$ and $f'_\epsilon(\lambda(\epsilon))$ on a small ϵ near the zero, that is, $f'_\epsilon(\lambda) \cdot (x - f_\epsilon(\lambda)) = f'_\epsilon(\lambda) \cdot x = 0$ by the same argument in Lemma 1. Then, we define a map $F : [-1, 1] \times [0, 1] \rightarrow \mathbb{R}$ as $F(\epsilon, \lambda) = f'_\epsilon(\lambda) \cdot x$. F is a smooth function by Proposition 1. It follows by the definition of $B(\zeta)$ that

$$\frac{\partial}{\partial \lambda} F(\epsilon, \lambda) \Big|_{(0, \lambda_f)} = f''(\lambda_f) \cdot x \neq 0.$$

By implicit function theorem, for each $x \in A \cap B(\zeta)$, $\lambda(\epsilon) = \lambda_{f_\epsilon}(x)$ is a smooth function for ϵ and $F(\epsilon, \lambda(\epsilon)) = 0$ in an open interval containing zero. Next, in order to prove uniform boundedness of $\frac{\partial \lambda(\epsilon)}{\partial \epsilon}$, we should verify that $f''_\epsilon(\lambda_{f_\epsilon}(x))$ uniformly converge to $f''(\lambda_f(x))$ on $A \cap B(\zeta)$ as ϵ goes to 0. First of all, for each λ , we have

$$\begin{aligned} f_{\epsilon_0}(\lambda) &= f(\lambda) + \int_0^{\epsilon_0} g(\epsilon, \lambda) d\epsilon \Rightarrow f''_{\epsilon_0}(\lambda) = f''(\lambda) + \int_0^{\epsilon_0} g''(\epsilon, \lambda) d\epsilon \\ &\Rightarrow \|f''_{\epsilon_0}(\lambda) - f''(\lambda)\| \leq \int_0^{\epsilon_0} \|g''(\epsilon, \lambda)\| d\epsilon \leq \epsilon_0 \cdot M, \end{aligned} \quad (11)$$

for some $M > 0$. Note that the above derivatives are differentiation by λ . Also, the second equation holds since $g(\epsilon, \cdot)$ is a twice continuously differentiable function for all ϵ ; thus, it is able to change the order of derivative and the integration. The last inequality holds because $g''(\epsilon, \lambda) (= \frac{\partial^2 g(\epsilon, \lambda)}{\partial \lambda^2})$ is continuous on $[-1, 1] \times [0, 1]$. Hence, it follows that

$$\begin{aligned} \|f''_\epsilon(\lambda_{f_\epsilon}(x)) - f''(\lambda_f(x))\| &\leq \|f''_\epsilon(\lambda_{f_\epsilon}(x)) - f''(\lambda_{f_\epsilon}(x))\| + \|f''(\lambda_{f_\epsilon}(x)) - f''(\lambda_f(x))\| \\ &\rightarrow 0, \end{aligned}$$

as $\epsilon \rightarrow 0$ uniformly on $x \in A \cap B(\zeta)$, because the first term uniformly converges to 0 by (11) and the last one also converges to 0 uniformly by Proposition 4 and the boundedness of f''' . We have that $|x \cdot f''(\lambda_f(x))| > \zeta$ owing to $x \in B(\zeta)$, and from (12), there exists

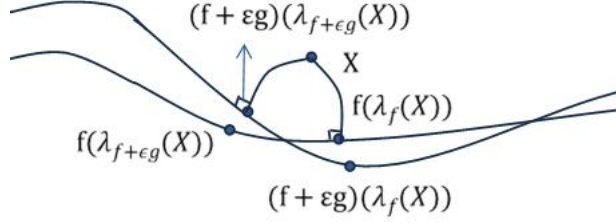


Figure 15: Two curves are on a spherical surface and the lines orthogonal to the curves denote the shortest geodesics.

a constant $\delta > 0$ such that $|\epsilon| < \delta \Rightarrow |x \cdot f''_{\epsilon}(\lambda_{f_{\epsilon}}(x))| \geq \frac{\zeta}{2}$. Since $f_{\epsilon}(\lambda) = f(\epsilon, \lambda)$ has continuous second partial derivatives, it is able to change the order of partial derivatives by Schwarz's theorem, as

$$\begin{aligned} \frac{\partial}{\partial \epsilon} \Big|_{\epsilon=\epsilon_0} f'_{\epsilon}(\lambda(\epsilon_0)) &= \frac{\partial}{\partial \epsilon} \Big|_{\epsilon=\epsilon_0} \frac{\partial}{\partial \lambda} \Big|_{\lambda=\lambda(\epsilon_0)} f_{\epsilon}(\lambda) \\ &= \frac{\partial}{\partial \lambda} \Big|_{\lambda=\lambda(\epsilon_0)} \frac{\partial}{\partial \epsilon} \Big|_{\epsilon=\epsilon_0} f_{\epsilon}(\lambda) \\ &= g'(\epsilon_0, \lambda(\epsilon_0)), \end{aligned}$$

for all $|\epsilon_0| < \delta$. Therefore, if $|\epsilon_0| < \delta$ by applying implicit function theorem to F again, then we obtain that $\lambda(\epsilon)$ is differentiable at $\epsilon = \epsilon_0$ and

$$\begin{aligned} |\lambda'(\epsilon_0)| &= \left| \frac{-\partial F(\epsilon, \lambda)/\partial \epsilon}{\partial F(\epsilon, \lambda)/\partial \lambda} \Big|_{(\epsilon_0, \lambda(\epsilon_0))} \right| = \frac{\left| x \cdot \frac{\partial}{\partial \epsilon} \Big|_{\epsilon=\epsilon_0} f'_{\epsilon}(\lambda(\epsilon_0)) \right|}{\left| x \cdot f''_{\epsilon_0}(\lambda(\epsilon_0)) \right|} \\ &\leq \frac{\|g'\|}{\zeta/2} \leq \frac{2}{\zeta}, \end{aligned}$$

which completes the proof. □

Proof of Theorem 1

Proof. If $f = h$, then nothing to prove. Thus, we assume that the curves f and $f + g (= h)$ are not identical and further both are parameterized by $\lambda \in [0, 1]$. To prove the result, we need to show that the conditional expectation is zero after exchanging the order of the derivative and expectation.

First, for order exchange, it is necessary to show that the following random variable

$$\begin{aligned} Z_\epsilon(X) &= \frac{\cos(d_{Geo}(X, f + \epsilon g)) - \cos(d_{Geo}(X, f))}{\epsilon} \\ &= \frac{\cos(d_{Geo}(X, (f + \epsilon g)(\lambda_{f+\epsilon g}(X)))) - \cos(d_{Geo}(X, f(\lambda_f(X))))}{\epsilon} \end{aligned} \quad (12)$$

is uniformly bounded for any sufficiently small $\epsilon > 0$. Then we apply bounded convergence theorem. Since the projection index of X represents the closest point in the curve, it follows that

$$Z_\epsilon(X) \leq \frac{\cos(d_{Geo}(X, (f + \epsilon g)(\lambda_{f+\epsilon g}(X)))) - \cos(d_{Geo}(X, f(\lambda_{f+\epsilon g}(X))))}{\epsilon}. \quad (13)$$

For simplicity, let $f_g(\lambda_\epsilon) := (f + g)(\lambda_{f+g}(X))$, $f_\epsilon(\lambda_\epsilon) := (f + \epsilon g)(\lambda_{f+\epsilon g}(X))$ and $f(\lambda_\epsilon) := f(\lambda_{f+\epsilon g}(X))$. By applying Lemma 3 to $\cos(d_{Geo}(X, f_\epsilon(\lambda_\epsilon)))$, as shown in Figure 15, the inequality of (13) becomes

$$\begin{aligned} Z_\epsilon(X) &\leq \frac{\cos(d_{Geo}(X, f_\epsilon(\lambda_\epsilon))) - \cos(d_{Geo}(X, f(\lambda_\epsilon)))}{\epsilon} \\ &= \frac{\cos(d_{Geo}(X, f(\lambda_\epsilon)))(\cos(d_{Geo}(f_\epsilon(\lambda_\epsilon), f(\lambda_\epsilon))) - 1) + (f(\lambda_\epsilon) \times f_\epsilon(\lambda_\epsilon)) \cdot (f(\lambda_\epsilon) \times X)}{\epsilon} \quad (14) \\ &= \frac{\cos(d_{Geo}(X, f(\lambda_\epsilon)))(\cos(\epsilon d_{Geo}(f_g(\lambda_\epsilon), f(\lambda_\epsilon))) - 1) + A_\epsilon(f(\lambda_\epsilon) \times f_g(\lambda_\epsilon)) \cdot (f(\lambda_\epsilon) \times X)}{\epsilon}, \end{aligned}$$

where $A_\epsilon = |f(\lambda_\epsilon) \times f_\epsilon(\lambda_\epsilon)|/|f(\lambda_\epsilon) \times f_g(\lambda_\epsilon)| = \sin(\epsilon d_{Geo}(f(\lambda_\epsilon), f_g(\lambda_\epsilon)))/|f(\lambda_\epsilon) \times f_g(\lambda_\epsilon)|$. The last equality is done by Definition 1. To get the upper bound of $Z_\epsilon(X)$, we further use the following fact, $|\frac{\sin \epsilon C}{\epsilon}| \leq |C|$ and $|\frac{1 - \cos \epsilon C}{\epsilon}| \leq \frac{|\epsilon| C^2}{2}$ for $C \in \mathbb{R}$ and $\epsilon \in \mathbb{R}$. Then, we have

$$Z_\epsilon(X) \leq \left| \cos(d_{Geo}(X, f(\lambda_\epsilon))) \right| \frac{|\epsilon| B^2}{2} + \frac{B}{|f(\lambda_\epsilon) \times f_g(\lambda_\epsilon)|} |(f(\lambda_\epsilon) \times f_g(\lambda_\epsilon)) \cdot (f(\lambda_\epsilon) \times X)|,$$

where $B = d_{Geo}(f(\lambda_\epsilon), f_g(\lambda_\epsilon)) \leq \|g\| < \pi$. Note that any smallest geodesic distance on a unit sphere is smaller than π . In addition, we can assume that ϵ is less than $1/\pi$ because we are only interested in ϵ near 0. Thus, we obtain the upper bound of $Z_\epsilon(X)$ in (14)

$$Z_\epsilon(X) \leq \frac{\pi}{2} + \pi = \frac{3\pi}{2}.$$

A lower bound of $Z_\epsilon(X)$ can be similarly obtained. Let $f_g(\lambda) := (f + g)(\lambda_f(X))$, $f_\epsilon(\lambda) :=$

$(f + \epsilon g)(\lambda_f(X))$ and $f(\lambda) := f(\lambda_f(X))$. By following the same path, we have

$$\begin{aligned} Z_\epsilon(X) &\geq \frac{\cos(d_{Geo}(X, (f + \epsilon g)(\lambda_f(X)))) - \cos(d_{Geo}(X, f(\lambda_f(X))))}{\epsilon} \\ &= \frac{\cos(d_{Geo}(X, f(\lambda)))(\cos(d_{Geo}(f_\epsilon(\lambda), f(\lambda))) - 1) + (f(\lambda) \times f_\epsilon(\lambda)) \cdot (f(\lambda) \times X)}{\epsilon} \quad (15) \\ &= \frac{\cos(d_{Geo}(X, f(\lambda)))(\cos(\epsilon d_{Geo}(f_g(\lambda), f(\lambda))) - 1) + B_\epsilon(f(\lambda) \times f_g(\lambda)) \cdot (f(\lambda) \times X)}{\epsilon}, \end{aligned}$$

where $B_\epsilon = |f(\lambda) \times f_\epsilon(\lambda)|/|f(\lambda) \times f_g(\lambda)| = \sin(\epsilon d_{Geo}(f(\lambda), f_g(\lambda)))/|f(\lambda) \times f_g(\lambda)|$. By the same way, it can be shown that

$$Z_\epsilon(X) \geq -\frac{3\pi}{2}.$$

Hence, we show that

$$|Z_\epsilon(X)| \leq \frac{3\pi}{2},$$

which is bounded for any $|\epsilon| \leq 1/\pi$. Then, by the bounded convergence theorem, it follows that

$$\left. \frac{dE_X \cos(d_{Geo}(X, f + \epsilon g))}{d\epsilon} \right|_{\epsilon=0} = E_X \left. \frac{d \cos(d_{Geo}(X, f + \epsilon g))}{d\epsilon} \right|_{\epsilon=0}.$$

Thus, the proof is completed provided that the following equation holds

$$E_{X| \cdot} \left(\left. \frac{d \cos(d_{Geo}(X, f + \epsilon g))}{d\epsilon} \right|_{\epsilon=0} \middle| \lambda_f(X) = \lambda \right) = 0, \text{ for a.e. } \lambda.$$

By the definition of derivative,

$$\left. \frac{d \cos(d_{Geo}(X, f + \epsilon g))}{d\epsilon} \right|_{\epsilon=0} = \lim_{\epsilon \rightarrow 0} Z_\epsilon(X),$$

and as shown, $Z_\epsilon(X)$ is bounded. Since f and $f + g$ are continuous, by Proposition 3, if X is not an ambiguity point of f and $f + g$, then

$$\lim_{\epsilon \rightarrow 0} f_g(\lambda_\epsilon) = f_g(\lambda), \quad \lim_{\epsilon \rightarrow 0} f(\lambda_\epsilon) = f(\lambda).$$

Next, to show the limit of Z_ϵ , we use the fact that $\lim_{\epsilon \rightarrow 0} \frac{\sin \epsilon C}{\epsilon} = C$ and $\lim_{\epsilon \rightarrow 0} \frac{1 - \cos \epsilon C}{\epsilon} = 0$ for $C \in \mathbb{R}$ and $\epsilon \in \mathbb{R}$. When $f_g(\lambda) \neq f(\lambda)$, it follows that

$$\lim_{\epsilon \rightarrow 0} \text{RHS of (14)} = d_{Geo}(f(\lambda), f_g(\lambda)) \frac{f(\lambda) \times f_g(\lambda)}{|f(\lambda) \times f_g(\lambda)|} \cdot (f(\lambda) \times X) = \mu(\lambda) \cdot (f(\lambda) \times X),$$

where $\mu(\lambda) = d_{Geo}(f(\lambda), f_g(\lambda))(f(\lambda) \times f_g(\lambda))/|f(\lambda) \times f_g(\lambda)|$ if $f(\lambda) \neq (f+g)(\lambda)$ and $\mu(\lambda) = 0$ otherwise. Similarly, we obtain that

$$\lim_{\epsilon \rightarrow 0} \text{RHS of (15)} = \mu(\lambda) \cdot (f(\lambda) \times X).$$

In summary, if X is not an ambiguity point of f and $f+g$, and $f(\lambda_f(X)) \neq (f+g)(\lambda_f(X))$, then we have

$$\left. \frac{d \cos(d_{Geo}(X, f + \epsilon g))}{d\epsilon} \right|_{\epsilon=0} = \mu(\lambda_f(X)) \cdot (f(\lambda_f(X)) \times X). \quad (16)$$

In the case of $f(\lambda_f(X)) = (f+g)(\lambda_f(X))$, the equation (16) also hold because its left and right hand side are 0. From Proposition 4, the limit of (16) is established for a.e. X . Since X is a random vector, $\lambda_f(X)$ is also a random variable depending on X . Thus, the following equality holds

$$E_X \left(\left. \frac{d \cos(d_{Geo}(X, f + \epsilon g))}{d\epsilon} \right|_{\epsilon=0} \right) = E_X \left(\mu(\lambda_f(X)) \cdot (f(\lambda_f(X)) \times X) \right). \quad (17)$$

Finally, if f is an extrinsic principal curve, then

$$E_{X| \cdot} (X | \lambda_f(X) = \lambda) = cf(\lambda)$$

for $\exists c \in \mathbb{R}$, and hence, it follows that

$$\begin{aligned} E_{X| \cdot} (\mu(\lambda_f(X)) \cdot (f(\lambda_f(X)) \times X) | \lambda_f(X) = \lambda) &= E_{X| \cdot} (\mu(\lambda) \cdot (f(\lambda) \times X) | \lambda_f(X) = \lambda) \\ &= \mu(\lambda) \cdot (f(\lambda) \times cf(\lambda)) = 0. \end{aligned}$$

Hence, we have

$$\text{LHS of (17)} = E_X (\mu(\lambda) \cdot (f(\lambda) \times X)) = E_\lambda [E_{X| \cdot} (\mu(\lambda) \cdot (f(\lambda) \times X) | \lambda_f(X) = \lambda)] = 0.$$

To prove the converse, we assume that $E_\lambda [E_{X| \cdot} (\mu(\lambda) \cdot (f(\lambda) \times X) | \lambda_f(X) = \lambda)] = E_\lambda [\mu(\lambda) \cdot E_{X| \cdot} (f(\lambda) \times X | \lambda_f(X) = \lambda)] = 0$ for all smooth $f+g$ satisfying $\|g\| \neq \pi$ and $\|g'\| \leq 1$. Since $f+g$ is only included in $\mu(\lambda)$, it followed that

$$E_{X| \cdot} (f(\lambda) \times X | \lambda_f(X) = \lambda) = f(\lambda) \times E_{X| \cdot} (X | \lambda_f(X) = \lambda) = 0 \quad \text{for a.e. } \lambda.$$

Therefore, we have

$$E_{X| \cdot} (X | \lambda_f(X) = \lambda) = cf(\lambda)$$

for $\exists c \geq 0$, which completes the proof. \square

Proof of Theorem 2

Proof. In the case of $f = h$, the result is obvious. We thus assume that f and $f + g (= h)$ are not identical. Further, suppose that $X \in A \cap B(\zeta)$ for a small $\zeta > 0$ and $\lambda_f(X) \in (0, 1)$ for a.e X . As the proof of Theorem 1, we use the bounded convergence theorem to change the order of derivative and expectation. For this purpose, we define

$$\begin{aligned} Z_\epsilon(X) &= \frac{d_{Geo}^2(X, f + \epsilon g) - d_{Geo}^2(X, f)}{\epsilon} \\ &= \frac{d_{Geo}^2(X, f_\epsilon(\lambda_{f_\epsilon})) - d_{Geo}^2(X, f(\lambda_f))}{\epsilon}, \end{aligned}$$

where $f_\epsilon := f + \epsilon g$ for $|\epsilon| \leq 1$. Let $\theta(\lambda, X)$ be a smaller angle between segments of geodesics from $f(\lambda)$ to X and from $f(\lambda)$ to $(f + g)(\lambda)$. Then, from Lemma 3, it follows that

$$\begin{aligned} F(\epsilon) := \cos(d_{Geo}(X, f_\epsilon(\lambda_{f_\epsilon}))) &= \cos(d_{Geo}(X, f(\lambda_{f_\epsilon}))) \cdot \cos(\epsilon \|g(\lambda_{f_\epsilon})\|) \\ &\quad + \sin(d_{Geo}(X, f(\lambda_{f_\epsilon}))) \cdot \sin(\epsilon \|g(\lambda_{f_\epsilon})\|) \cdot \cos(\theta(\lambda_{f_\epsilon}, X)), \end{aligned}$$

where $\|g(\lambda)\| = d_{Geo}(f(\lambda), (f + g)(\lambda)) < \pi$.

Firstly, we verify that $Z_\epsilon(X)$ is uniformly bounded for a small $\epsilon > 0$. By Lemma 5, there are constants $C > 0$ and $\eta > 0$ such that if $|\epsilon_0| < \eta$, then $\lambda(\epsilon)$ is differentiable at $\epsilon = \epsilon_0$ and $|\frac{\partial \lambda(\epsilon)}{\partial \epsilon}|_{\epsilon=\epsilon_0}| < C$, where $\lambda(\epsilon) = \lambda_{f_\epsilon}(X)$. For simplicity of notation, let $\lambda_{f_\epsilon}(X) = \lambda_\epsilon$ and $\lambda_f(X) = \lambda_0$. If $0 < |\epsilon_0| < \eta$, then by triangle inequality on sphere and mean value theorem, it follows that

$$\begin{aligned} |Z_{\epsilon_0}(X)| &= \left| \frac{d_{Geo}(X, f_{\epsilon_0}(\lambda_{f_{\epsilon_0}})) - d_{Geo}(X, f(\lambda_f))}{\epsilon_0} \right| \cdot \left(d_{Geo}(X, f_{\epsilon_0}(\lambda_{f_{\epsilon_0}})) + d_{Geo}(X, f(\lambda_f)) \right) \\ &\leq 2\pi \cdot \frac{d_{Geo}(f(\lambda_0), f_{\epsilon_0}(\lambda_{\epsilon_0}))}{\epsilon_0} \\ &\leq 2\pi \cdot \frac{d_{Geo}(f(\lambda_0), f(\lambda_{\epsilon_0})) + d_{Geo}(f(\lambda_{\epsilon_0}), f_{\epsilon_0}(\lambda_{\epsilon_0}))}{\epsilon_0} \\ &< 2\pi \cdot \left(s \cdot \frac{\|\lambda_0 - \lambda_{\epsilon_0}\|}{\epsilon_0} + \|g(\lambda_{\epsilon_0})\| \right) \\ &\leq 2\pi \cdot (s \cdot C + \pi), \end{aligned}$$

where $s := |f'(\lambda)|$ for all λ . Therefore, $Z_\epsilon(X)$ is uniformly bounded on $X \in A \cap B(\zeta)$ for $0 < |\epsilon| < \eta$.

Secondly, we find the limit of $Z_\epsilon(X)$. For this purpose, we define a map $u : (-1, 1] \rightarrow (1, \infty)$ by $u(x) = \arccos(x) \cdot \frac{1}{\sqrt{1-x^2}}$ if $x \in (-1, 1)$, and $u(1) = 1$. By simple calculations, u is a monotone decreasing continuous function on $(-1, 1]$. Note that $F(\epsilon)$ is differentiable for $|\epsilon| < \eta$. By the mean value theorem to find the limit of $Z_\epsilon(X)$, we have

$$\begin{aligned} Z_{\epsilon_0}(X) &= \frac{d_{Geo}^2(X, f_{\epsilon_0}(\lambda_{f_{\epsilon_0}})) - d_{Geo}^2(X, f(\lambda_f))}{\epsilon_0} \\ &= \frac{\arccos^2(F(\epsilon_0)) - \arccos^2(F(0))}{\epsilon_0} \\ &= -2 \arccos(F(\epsilon_1)) \cdot \frac{1}{\sqrt{1-F^2(\epsilon_1)}} \cdot \frac{dF(\epsilon)}{d\epsilon} \Big|_{\epsilon=\epsilon_1} \end{aligned} \quad (18)$$

for $0 < |\epsilon_1| < |\epsilon_0| < \eta$. When $F(\epsilon_1) = 1$, the last equality is considered as a limit that is well-defined, because $\lim_{x \rightarrow 1} u(x) = 1$ and $u(x)$ is smoothly extended on an open interval containing 1 such that $u(x)$ is differentiable at $x = 1$. By applying chain rule to the derivative of F , we obtain

$$\begin{aligned} \lim_{\epsilon_0 \rightarrow 0} \frac{\partial F(\epsilon)}{\partial \epsilon} \Big|_{\epsilon=\epsilon_0} &= \lim_{\epsilon_0 \rightarrow 0} \left[\sin(d_{Geo}(X, f(\lambda_{f_{\epsilon_0}}))) \cdot \cos(\theta(\lambda_{f_{\epsilon_0}}, X)) \cdot (\|g(\lambda_{f_{\epsilon_0}})\| + \epsilon_0 \cdot \frac{\partial \|g(\lambda_{f_{\epsilon_0}})\|}{\partial \epsilon} \Big|_{\epsilon=\epsilon_0}) \right] \\ &\quad - \lim_{\epsilon_0 \rightarrow 0} \left[\sin(d_{Geo}(X, f(\lambda_{f_{\epsilon_0}}))) \cdot \frac{\partial d_{Geo}(X, f(\lambda_{f_{\epsilon_0}}))}{\partial \epsilon} \Big|_{\epsilon=\epsilon_0} \right]. \end{aligned}$$

In addition,

$$\frac{\partial \|g(\lambda_{f_{\epsilon_0}})\|}{\partial \epsilon} \Big|_{\epsilon=\epsilon_0} = \frac{\partial \|g(\lambda)\|}{\partial \lambda} \Big|_{\lambda=\lambda_{f_{\epsilon_0}}} \frac{\partial \lambda(\epsilon)}{\partial \epsilon} \Big|_{\epsilon=\epsilon_0},$$

which exists and does not diverge as ϵ_0 goes to 0, since $\|g(\lambda)\| = d_{Geo}(f(\lambda), (f+g)(\lambda))$ is continuously differentiable for λ and $\frac{\partial \lambda(\epsilon)}{\partial \epsilon} \Big|_{\epsilon=0}$ is bounded by Lemma 5. Moreover,

$$\begin{aligned} \lim_{\epsilon_0 \rightarrow 0} \frac{\partial d_{Geo}(X, f(\lambda_{f_{\epsilon_0}}))}{\partial \epsilon} \Big|_{\epsilon=\epsilon_0} &= \lim_{\epsilon_0 \rightarrow 0} \frac{\partial d_{Geo}(X, f(\lambda))}{\partial \lambda} \Big|_{\lambda=\lambda_{f_{\epsilon_0}}} \frac{\partial \lambda(\epsilon)}{\partial \epsilon} \Big|_{\epsilon=\epsilon_0} \\ &= \frac{\partial d_{Geo}(X, f(\lambda))}{\partial \lambda} \Big|_{\lambda=\lambda_f} \frac{\partial \lambda(\epsilon)}{\partial \epsilon} \Big|_{\epsilon=0} \\ &= 0, \end{aligned}$$

where $\lambda(\epsilon) = \lambda_{f_{\epsilon}}$. The last equality is done by the definition of λ_f . Therefore, we have

$$\lim_{\epsilon \rightarrow 0} \frac{\partial F(\epsilon)}{\partial \epsilon} = \|g(\lambda_f)\| \cdot \cos(\theta(\lambda_f, X)) \cdot \sin(d_{Geo}(X, f(\lambda_f))). \quad (19)$$

Thirdly, it follows from (18) and (19) that

$$\begin{aligned}\lim_{\epsilon_0 \rightarrow 0} Z_{\epsilon_0}(X) &= \lim_{\epsilon_1 \rightarrow 0} \left[-2 \arccos F(\epsilon_1) \cdot \frac{1}{\sqrt{1-F^2(\epsilon_1)}} \cdot \frac{dF(\epsilon)}{d\epsilon} \Big|_{\epsilon=\epsilon_1} \right] \\ &= -2u \left(\cos(d_{Geo}(X, f(\lambda_f))) \right) \cdot \|g(\lambda_f)\| \cdot \cos(\theta(\lambda_f, X)) \cdot \sin(d_{Geo}(X, f(\lambda_f)))\end{aligned}\quad (20)$$

$$\begin{aligned}&= -2d_{Geo}(X, f(\lambda_f)) \cdot \frac{1}{\sin(d_{Geo}(X, f(\lambda_f)))} \cdot \|g(\lambda_f)\| \cdot \cos(\theta(\lambda_f, X)) \cdot \sin(d_{Geo}(X, f(\lambda_f))) \\ &= -2d_{Geo}(X, f(\lambda_f)) \cdot \|g(\lambda_f)\| \cdot \cos(\theta(\lambda_f, X)),\end{aligned}\quad (21)$$

In the case of $d_{Geo}(X, f(\lambda_f)) = 0$, the same result follows since both (20) and (21) are zero. Thus, by Proposition 5, the equation (21) is established for a.e $X \in B(\zeta)$. Next, we notice that, for a smooth curve f , it can be shown that $M_\lambda := \{x \in S^2 | \lambda_f(x) = \lambda\}$ is a subset of the great circle perpendicular to f at $f(\lambda)$ by Lemma 2. Let S_λ be the great circle perpendicular to f at $f(\lambda)$. That is, $M_\lambda \subset S_\lambda \cong S^1$. Moreover, a connected proper subset of S_λ is isometric to a line with the same length in \mathbb{R} , which makes the intrinsic mean on M_λ feasible. Thus, f is an intrinsic principal curve of X , by the definition of $\theta(\lambda_f, X)$ and $\cos(\pi - \theta) = -\cos(\theta)$, if and only if

$$E_{X| \cdot} \left(d_{Geo}(X, f(\lambda_f)) \cdot \cos(\theta(\lambda_f, X)) | \lambda_f(X) = \lambda \right) = 0 \text{ for a.e. } \lambda.$$

Finally, it follows from (21) and bounded convergence theorem that

$$\begin{aligned}\frac{dE_X d_{Geo}^2(X, f + \epsilon g)}{d\epsilon} \Big|_{\epsilon=0} &= \lim_{\epsilon \rightarrow 0} \frac{E_X d_{Geo}^2(X, f + \epsilon g) - E_X d_{Geo}^2(X, f)}{\epsilon} \\ &= E_X \left[\lim_{\epsilon \rightarrow 0} \frac{d_{Geo}^2(X, f + \epsilon g) - d_{Geo}^2(X, f)}{\epsilon} \right] \\ &= E_\lambda \left[E_{X| \cdot} \left(\lim_{\epsilon \rightarrow 0} Z_\epsilon(X) | \lambda_f(X) = \lambda \right) \right] \\ &= -2E_\lambda \left[E_{X| \cdot} \left(d_{Geo}(X, f(\lambda_f(X))) \cdot \|g(\lambda_f(X))\| \cdot \cos(\theta(\lambda_f, X)) | \lambda_f(X) = \lambda \right) \right] \\ &= -2E_\lambda \left[\|g(\lambda)\| \cdot E_{X| \cdot} \left(d_{Geo}(X, f(\lambda_f(X))) \cdot \cos(\theta(\lambda_f, X)) | \lambda_f(X) = \lambda \right) \right] \\ &= 0.\end{aligned}$$

Conversely, we assume that

$$E_\lambda \left[\|g(\lambda)\| \cdot E_{X| \cdot} \left(d_{Geo}(X, f(\lambda_f)) \cdot \cos(\theta(\lambda_f, X)) | \lambda_f(X) = \lambda \right) \right] = 0,$$

for all $f + g(=h)$ such that $\|g\| \neq \pi$ and $\|g'\| \leq 1$. Then, we have

$$E_{X| \cdot} \left(d_{Geo}(X, f(\lambda_f)) \cdot \cos(\theta(\lambda_f, X)) | \lambda_f(X) = \lambda \right) = 0 \text{ for a.e. } \lambda,$$

which is equivalent to that f is an intrinsic principal curve of X . \square

Proof of Theorem 3

Proof. The proof follows the same line of Theorem 2. For given $h \neq f$, we assume that $X \in A \cap B(\zeta)$ for a small $\zeta > 0$ and $\lambda_f(X) \in (0, 1)$ for a.e. X . By Lemma 5, there are constants $C > 0$ and $\eta > 0$ such that if $|\epsilon_0| < \eta$, then $\lambda(\epsilon)$ is differentiable at $\epsilon = \epsilon_0$ and $|\frac{\partial \lambda(\epsilon)}{\partial \epsilon}|_{\epsilon=\epsilon_0}| < C$, where $\lambda(\epsilon) = \lambda_{f_\epsilon}(X)$. For simplicity, let $\lambda_{f_\epsilon}(X) = \lambda_\epsilon$ and $\lambda_f(X) = \lambda_0$. If $0 < |\epsilon_0| < \eta$, by similar arguments in Theorem 2 we obtain

$$\begin{aligned} |Z_{\epsilon_0}(X)| &= \left| \frac{d_{Geo}(X, f_{\epsilon_0}(\lambda_{f_{\epsilon_0}})) - d_{Geo}(X, f(\lambda_f))}{\epsilon_0} \right| \\ &\leq \left| \frac{d_{Geo}(f(\lambda_0), f_{\epsilon_0}(\lambda_{\epsilon_0}))}{\epsilon_0} \right| \\ &\leq \left| \frac{d_{Geo}(f(\lambda_0), f(\lambda_{\epsilon_0})) + d_{Geo}(f(\lambda_\epsilon), f_{\epsilon_0}(\lambda_{\epsilon_0}))}{\epsilon_0} \right| \\ &\leq s \cdot \frac{\|\lambda_0 - \lambda_{\epsilon_0}\|}{\epsilon_0} + \|g(\lambda_{\epsilon_0})\|, \\ &\leq s \cdot C + \pi, \end{aligned}$$

where $s := |f'(\lambda)|$ for all λ . The last inequality is done by mean value theorem. That is, $Z_\epsilon(X)$ is uniformly bounded on $X \in A \cap B(\zeta)$ for $0 < |\epsilon| < \eta$. Recall that, in the proof of Theorem 2, we have verified that

$$\lim_{\epsilon \rightarrow 0} \frac{\partial F(\epsilon)}{\partial \epsilon} = \|g(\lambda_f)\| \cdot \cos(\theta(\lambda_f, X)) \cdot \sin(d_{Geo}(X, f(\lambda_f))).$$

By mean value theorem, for $0 < |\epsilon_0| < \eta$, we obtain that

$$\begin{aligned} Z_{\epsilon_0}(X) &= \frac{d_{Geo}(X, f_{\epsilon_0}(\lambda_{f_{\epsilon_0}})) - d_{Geo}(X, f(\lambda_f))}{\epsilon_0} \\ &= \frac{\arccos(F(\epsilon_0)) - \arccos(F(0))}{\epsilon_0} \\ &= -\frac{1}{\sqrt{1 - F^2(\epsilon_1)}} \cdot \frac{dF(\epsilon)}{d\epsilon} \Big|_{\epsilon=\epsilon_1}, \end{aligned}$$

where $0 < |\epsilon_1| < |\epsilon_0|$. Hence, it follows that

$$\begin{aligned}
\lim_{\epsilon_0 \rightarrow 0} Z_{\epsilon_0}(X) &= \lim_{\epsilon_1 \rightarrow 0} \left[- \frac{1}{\sqrt{1 - F^2(\epsilon_1)}} \cdot \frac{dF(\epsilon)}{d\epsilon} \Big|_{\epsilon=\epsilon_1} \right] \\
&= - \frac{1}{\sin(d_{Geo}(X, f(\lambda_f)))} \cdot \|g(\lambda_f)\| \cdot \cos(\theta(\lambda_f, X)) \cdot \sin(d_{Geo}(X, f(\lambda_f))) \\
&= - \|g(\lambda_f)\| \cdot \cos(\theta(\lambda_f, X)), \tag{22}
\end{aligned}$$

where the equation (22) holds for $X \in A \cap B(\zeta)$ such that $d_{Geo}(X, f(\lambda_f)) > 0$. Because the trajectory of f , $\{f(\lambda) \in S^2 \mid \lambda \in [0, 1]\}$, is a measure zero set by Lemma 4, the equation (22) holds for a.e $X \in B(\zeta)$ by Proposition 4. Moreover, f is a median principal curve of X if and only if

$$E_{X| \cdot} \left(\text{sgn}(\cos(\theta(\lambda_f, X))) \mid \lambda_f(X) = \lambda \right) = 0 \text{ for a.e. } \lambda,$$

where $\text{sgn}(x) = 1$ if $x \geq 0$ and otherwise -1. Finally, the result can be obtained in a similar manner to the proofs of Theorem 1 and 2 by applying (22) and bounded convergence theorem. The converse is further proved in the same way as the proofs of Theorem 1 and 2.

□

References

- Bajaj, C. (1988). The algebraic degree of geometric optimization problems. *Discrete Computational Geometry*, **3**, 177–191.
- Banfield, J. D. and Raftery, A. E. (1992). Ice floe identification in satellite image using mathematical morphology and clustering about principal curves. *Journal of the American Statistical Association*, **87**, 7–16.
- Bhattacharya, R., Ellingson, L., Liu, X., Patrangenaru, V. and Crane, M. (2012). Extrinsic analysis on manifolds is computationally faster than intrinsic analysis with applications to quality control by machine vision. *Applied Stochastic Models in Business and Industry*, **28**, 222-235.

- Bhattacharya, R. and Patrangenaru, V. (2003). Large sample theory of intrinsic and extrinsic sample means on manifolds. Part I. *The Annals of Statistics*, **31**, 1–29.
- Bhattacharya, R. and Patrangenaru, V. (2005). Large sample theory of intrinsic and extrinsic sample means on manifolds. Part II. *The Annals of Statistics*, **33**, 1225–1259.
- Biau, G. and Fischer, A. (2012). Parameter selection for principal curves. *IEEE Transactions on Information Theory*, **58**, 1924–1939.
- Buss, S. R. and Fillmore, J. P. (2001). Spherical averages and applications to spherical splines and interpolation. *ACM Transactions on Graphics*, **20**, 95–126.
- Cippitelli, E., Gasparrini, S., Gambi, E. and Spinsante, S. (2016). A human activity recognition system using skeleton data from RGBD sensors. *Computational Intelligence and Neuroscience*, **2016**, Article ID 4351435.
- Fletcher, P. T., Lu, C., Pizer, S. M. and Joshi, S. (2004). Principal geodesic analysis for the study of nonlinear statistics of shape. *IEEE Transactions on Medical Imaging*, **23**, 995–1005.
- Fletcher, P. T., Venkatasubramanian, S. and Joshi, S. (2009). The geometric median on Riemannian manifolds with application to robust atlas estimation. *Neuroimage*, **45**, 143–152.
- Gray, N. H., Geiser, P. A. and Geiser, J. R. (1980). On the least-squares fit of small and great circles to spherically projected orientation data. *Journal of the International Association for Mathematical Geology*, **12**, 173–184.
- Hastie, T. and Stuetzle, W. (1989). Principal curves. *Journal of the American Statistical Association*, **84**, 502–516.
- Hauberg, S. (2016). Principal curves on Riemannian manifolds. *IEEE Transactions on Pattern Analysis and Machine Intelligence*, **38**, 1915–1921.

- Huckemann, S. and Ziezold, H. (2006). Principal component analysis for Riemannian manifolds with an application to triangular shape spaces. *Advances in Applied Probability*, **38**, 299–319.
- Huckemann, S., Hotz, T. and Munk, A. (2010). Intrinsic shape analysis: Geodesic PCA for Riemannian manifolds modulo isometric Lie group actions. *Statistica Sinica*, **20**, 1–58.
- Jung, S., Foskey, M. and Marron, J. S. (2011). Principal arc analysis on direct product manifolds. *The Annals of Applied Statistics*, **5**, 578–603.
- Jung, S., Dryden, I. M. and Marron, J. S. (2012). Analysis of principal nested spheres. *Biometrika*, **99**, 551–568.
- Le, H. and Kume, A. (2000). The Fréchet mean shape and the shape of the means. *Advances in Applied Probability*, **32**, 101–113.
- Panaretos, V. M., Pham, T. and Yao, Z. (2014). Principal flows. *Journal of the American Statistical Association*, **109**, 424–436.
- Pennec, X. (2006). Intrinsic statistics on Riemannian manifolds: Basic tools for geometric measurements. *Journal of Mathematical Imaging and Vision*, **25**, 127–154.
- Siddiqi, K. and Pizer, S. (2008). *Medial Representations: Mathematics, Algorithms and Applications*. Springer, New York.
- Srivastava, A. and Klassen, E. (2002). Monte Carlo extrinsic estimators of manifold-valued parameters. *IEEE Transactions on Signal Processing*, **50**, 299–308.
- Tibshirani, R. (1992). Principal curves revisited. *Statistics and Computing*, **2**, 183–190.